HHS Public Access

Author manuscript

*Toxicol Appl Pharmacol*. Author manuscript; available in PMC 2021 January 21.

Published in final edited form as:

*Toxicol Appl Pharmacol*. 2020 December 15; 409: 115282. doi:10.1016/j.taap.2020.115282.

# Biological effects of inhaled hydraulic fracturing sand dust. II. Particle characterization and pulmonary effects 30 d following intratracheal instillation

**Jeffrey S. Fedan**[a,*], **Ann F. Hubbs**[a], **Mark Barger**[a], **Diane Schwegler-Berry**[a], **Sherri A. Friend**[a], **Stephen S. Leonard**[a], **Janet A. Thompson**[a], **Mark C. Jackson**[a], **John E. Snawder**[a], **Alan K. Dozier**[a], **Jayme Coyle**[a], **Michael L. Kashon**[a], **Ju-Hyeong Park**[b], **Walter McKinney**[a], **Jenny R. Roberts**[a]

[a]Health Effects Laboratory Division, National Institute for Occupational Safety and Health, Morgantown, WV 26505, United States of America

[b]Respiratory Health Division, National Institute for Occupational Safety and Health, Morgantown, WV 26505, United States of America

## Abstract

Hydraulic fracturing ("fracking") is used in unconventional gas drilling to allow for the free flow of natural gas from rock. Sand in fracking fluid is pumped into the well bore under high pressure to enter and stabilize fissures in the rock. In the process of manipulating the sand on site, respirable dust (fracking sand dust, FSD) is generated. Inhalation of FSD is a potential hazard to workers inasmuch as respirable crystalline silica causes silicosis, and levels of FSD at drilling work sites have exceeded occupational exposure limits set by OSHA. In the absence of any information about its potential toxicity, a comprehensive rat animal model was designed to investigate the bioactivities of several FSDs in comparison to MIN-U-SIL® 5, a respirable α-quartz reference dust used in previous animal models of silicosis, in several organ systems (Fedan, J.S., Toxicol Appl Pharmacol. 00, 000–000, 2020). The present report, part of the larger investigation, describes: 1) a comparison of the physico-chemical properties of nine FSDs, collected at drilling sites, and MIN-U-SIL® 5, a reference silica dust, and 2) a comparison of the pulmonary inflammatory responses to intratracheal instillation of the nine FSDs and MIN-U-SIL® 5. Our findings indicate that, in many respects, the physico-chemical characteristics, and the biological effects of the FSDs and MIN-U-SIL® 5 after intratracheal instillation, have distinct differences.

[*]Corresponding author at: Health Effects Laboratory Division, National Institute for Occupational Safety and Health, 1000 Frederick Lane, Morgantown, WV 26508, United States of America. jsf2@cdc.gov (J.S. Fedan).



Declaration of Competing Interest

The authors declare that they have no conflicts of interest in relation to this publication.

Supplementary data to this article can be found online at https://doi.org/10.1016/j.taap.2020.115282.

**Keywords**

Fracking sand dust; Silica; MIN-U-SIL®; Particle characterization; Rat model

## 1. Introduction

Recently, concern has been raised about the possible public health effects associated with hydraulic fracturing (fracking) in the U.S. and elsewhere, in particular, the effects of respirable fracking sand dusts (FSDs) derived from the manipulation of sand at well sites. It has long been known that inhalation of α-quartz, a form of crystalline silica, is associated with the development of silicosis in many workplaces [Castranova et al., 1996; Silicosis and Silicate Disease Committee, 1988; National Institute for Occupational Safety and Health (NIOSH), 2002a, 2002b; Leung et al., 2012; Cohen et al., 2016]. However, information on the relative toxicities of dusts from FSDs containing crystalline silica is lacking.

This report is the second in a series of tandem papers in which the potential toxicity of FSDs was comprehensively investigated. The first paper in the series (Fedan, 2020) describes the overall approach to the investigation in the context of current knowledge about silica toxicity and research gaps. The other studies in this series have examined the effects of FSD on lung ventilatory and non-ventilatory functions, inflammatory mechanisms, and cardiovascular, immune and nervous systems and kidney (Russ et al., 2020; Anderson et al., 2020; Sager et al., 2020; Krajnak et al., 2020; Sriram et al., 2020) and cytotoxicity (Olgun et al., 2020), and have been summarized (Investigative Team, 2020).

It has been known for decades that that inhalation of crystalline silica, or dust containing crystalline silica, gives rise to silicosis, kidney disease, autoimmune disease, lung cancer and increased susceptibility to tuberculosis in workers (Department of Health and Human Services, 2002; McDonald et al., 2005). More recently, the advent of unconventional, horizontal drilling and fracking to obtain natural gas from subterranean rock formations has led to exposure of workers to FSD. The FSD arises from manipulation of sand at the drilling site that is included in the fracking fluid to stabilize induced fractures in the rock (as a fissure “proppant”) to increase porosity of the rock to facilitate extraction of gas and oil. Whereas much effort has been expended to model the pulmonary toxicity of inhaled, nearly pure respirable crystalline silica dust in animals [see, for example, Castranova et al., 2002 and Porter et al., 2002, 2004], nothing is known of the potential toxicity of FSD in humans or animals.

The purposes of the present study were 1) to characterize FSD particles and MIN-U-SIL® 5 (MIN-U-SIL) with respect to their physic-chemical properties, and 2) to obtain preliminary information on the comparative pulmonary toxicity of intratracheally-instilled FSDs and MIN-U-SIL, the former composed of non-respirable and respirable particles and latter which consists of nearly pure, respirable crystalline silica. One of the FSDs was used in animal inhalation exposures to assess potential toxicity in several organ systems (Fedan, 2020), the results of which are described in the papers referred to above.

## 2. Methods

### 2.1. FSDs and MIN-U-SIL

The FSDs used in this study were collected by commercial vacuum dust collection systems at fracking sites in the U.S. and were provided by industry partners or NIOSH field staff. These systems utilize a large 30,000 to 40,000 cfm central vacuum-baghouse connected via customizable ducts and shrouding to isolate and collect airborne dusts from primary FSD emission sources previously identified by NIOSH research (Esswein et al., 2013). FSDs were obtained from: Jackson County, TX; Washington County, TX; Fayette County, TX; Karnes County, TX; Bienville Parish, LA; DeWitt County, TX; Kingfisher County, OK; Washington County, PA; and Barbour County, WV.

The silica sample used in this study as a reference was MIN-U-SIL® 5 (U.S. Silica; Berkeley Springs, WV). It is a high-purity, high-quality, natural crystalline silica, 99.2% $SiO_2$ (claimed). At least 97% of the MIN-U-SIL silica particles have an equivalent spherical diameter < 5 μm.

All the FSDs and MIN-U-SIL were stored in air-tight containers and kept in a refrigerator. The dusts were not conditioned in any way.

### 2.2. Endotoxin analysis

Endotoxin analysis of each neat FSD and MIN-U-SIL was performed by Indoor Biotechnologies (Charlottesville, VA). The Endpoint Chromogenic Limulus Amebocyte Lysate (LAL) assay was used to quantitatively test for gram-negative bacterial endotoxin in the MIN-U-SIL and FSDs. The reporting limit was ~0.062 endotoxin units (EU)/mg. The limit of detection in one in-house sample was <1 EU/mg.

### 2.3. Particle size and physico-chemical characteristics of FSDs and MIN-U-SIL

The FSD and MIN-U-SIL particle sizes were measured in several ways. The nine FSDs and MIN-U-SIL were examined to compare their physico-chemical characteristics.

**2.3.1. Scanning electron microscopy (SEM)—**The sizes of FSDs and MIN-U-SIL particles were determined from examination of particles under the scanning electron microscope using two methods. In the first, an FSD sample was sonicated in isopropyl alcohol and filtered through 0.2 μm polycarbonate filters. A portion of the filter was cut, placed onto a carbon-taped stub, and carbon-coated. The sample was then examined using a Tescan (Warrendale, PA) SEM equipped with a Gresham light element detector and an IXRF digital imaging system. In the second method, samples were dispersed in double-distilled water and filtered with a 0.2 μm nucleopore filter. The filter was attached with double-stick carbon tape on an aluminum mount and sputter-coated with gold/palladium. Images were captured on a Hitachi S-4800 field-emission scanning electron microscope (Tokyo, Japan).

Particle sizes were estimated from SEM images on the live image screen of the Hitachi S4800 SEM. To establish a conversion factor, a metric ruler was used to measure the micron scale bar on the live image in mm. The same metric ruler was used to measure the individual particles in mm. The particles in the image field were assessed, and particles that were not

fully visible in the field were discarded. If the particles were found to have a length that was at least two times the width of the particle, it was measured for length and width. The particles that did not meet that criterion were measured using the area equivalent diameter technique where the widest portion of the particle was measured. When all measurements were taken, the mm values were converted back to microns.

**2.3.2. Energy dispersive analyses (EDS) and mapping—**EDS analysis permits definition of surface elements. EDS was performed in laboratories at NIOSH, Morgantown, WV and NIOSH, Cincinnati, OH.

EDS was used to characterize in three stages the elemental composition of individual FSD 8 particles that were ≤ 2 μm in size along their major axis. First, 200 FSD 8 particles were analyzed using an EDS detector pinpointing one location on the surface of a single particle, and particles were categorized based on similarity of elemental composition from measurements made in that one area. Subsequently, particles were examined in greater detail by directing the electron beam to several areas on the surface of a single particle. Then, a comprehensive element mapping of the nine FSDs and MIN-U-SIL particles was performed on populations of dust particles.

In FSD 9, unique particles were observed that appeared to be near perfect spheres. To further explore these particles, individual bulk FSD 9 samples (1 mg) were added to 10 ml of filtered distilled water, and vortexed for 30 s. One-half ml of the dust solution was dropped onto a 0.2 μ polycarbonate filter seated in a vacuum filtration unit, vacuum was applied, and the filter was removed after 30 s. After drying overnight, a wedge-shaped piece was cut from the round polycarbonate filter and mounted on a 13 mm aluminum stub using double stick carbon tape. The samples were coated with gold and palladium using the SPI sputter coating system (SPI Supplies; West Chester, PA) for 2 min. The samples were imaged using a Hitachi S4800 field emission SEM (Hitachi, Tokyo, Japan) at 20 KV. Regions of interest (ROI) were identified for high resolution digital imaging and EDS mapping using the Bruker Quantax detector (Madison, WI). Each ROI was mapped for 90 s. The generated images were pseudo-colorized based on the elemental composition. The map colors were auto-assigned by the software based on the most prevalent element in each ROI.

For EDS mapping of the nine FSDs and MIN-U-SIL, the dust samples were mounted on SEM stubs by first placing a conductive sticky carbon film on the stub. A small amount of sand was poured onto wax paper and the SEM stub was inverted and placed onto the sand. The sand readily adhered to the sticky carbon film with the sand grains being densely packed. Low magnification elemental mapping was used to obtain an overall picture of the sands' general compositions, using a Phenom XL SEM (ThermoFisher Scientific, Inc.) for imaging and elemental mapping. The SEM operates at 15 keV and has an energy dispersive spectrometer mounted internally.

Differences were observed in composition and particle sizes between the samples. The overall compositions were measured by adding all the EDS spectra gathered in each map and having those spectra quantized using software that came with the Phenom SEM. Anomalies were observed in the EDS spectra during the analysis. First, for most samples the

sulfur peak was a few volts off center in the EDS spectra. This indicates another peak is overlapping the sulfur peak from another element or it is not actually sulfur. Due to the limited energy range of the EDS spectra, because of the 15 keV operating voltage, it could not be determined which element was causing the overlap. Secondly, more than one spectrum had a small unidentified peak between potassium and calcium. This peak could not be identified without having the higher energy range of the EDS spectra present. Because this peak and the sulfur overlap peak were small, it would not affect the overall results that are presented here. It should also be noted that all the maps show shadowing effects due to the low take off angle of the EDS detector. These appear as gray areas behind large grains in the composite maps. The SEM is not equipped with a tilting stage to alleviate this shadowing effect.

**2.3.3. Dynamic light scattering (DLS)—**Particle sizes of dispersed FSDs and MIN-U-SIL were assessed using DLS. Ultrasonication dispersions of all FSD samples at a concentration of 1.67 mg/ml in phosphate-buffered saline (PBS) were briefly vortexed to homogenize the sample, and a sample was abstracted for assessment into a 1 cm cuvette. Hydrodynamic diameter measurements were performed using the Zetasizer Nano ZS (Malvern Pananalytical; Worcestershire, UK) at 25 °C. Intensity-based hydrodynamic diameter was converted to number distributions according to Mie theory using the Zetasizer DTS Software v. 7.12 (Malvern Pananalytical). [The intensity patterning over the time of measurement detected by the photodetector after having reflected light off a sample is used to calculate particle sizes based on the Stokes-Einstein equation. Mie theory is then applied to calculate number distributions.] For all samples, $SiO_2$ absorbance and refractive index was 0.010 and 1.450, respectively. Dispersant PBS refractive index and dynamic viscosity were 1.330 and 0.8820 centipose, respectively. Since DLS measurements were taken on a static suspension, sedimented particles would have not been included in size determination. For this reason, particle sizing as measured by this procedure would have been biased towards smaller particles that remained suspended during the measuring period.

**2.3.4. Qualitative X-ray diffraction (XRD) scan of FSDs—**XRD analysis was contracted to Bureau Veritas North America (BVNA). Samples were prepared and analyzed by XRD according to NIOSH Method 7500 (National Institute for Occupational Safety and Health, 2002b). Prior to the quantitative quartz analysis, the full spectra were used to qualitatively identify the mineral content (NIOSH 7500 Steps 4.a.). Then, the sample was prepared as described in NIOSH 7500 Step 4.b. using sieving to attain the less than 10 μm material. Briefly, the sample was placed in a fused corundum mortar. 2-Propanol (IPA) was added and the sample was stirred and mixed to suspend the particulates in the IPA. The coarse particulate was allowed to settle, and the fine particulate was decanted onto the 10 μm sieve. The remainder of the particulate was ground, and this process was repeated three times followed by a final rinse of the mortar with IPA. Approximately 2 mg of sieved and dried sample was then further prepared and analyzed quantitatively for silica. Full X-ray diffraction scans were performed with confirmation of quartz primary, secondary and tertiary peaks in order to identify and correct for mineral interferences. FSD 8 showed a particularly high calcium and iron content, which can create a high bias in the analysis for

quartz (Rosa Key-Schwartz, NIOSH, personal communication). NIST Certified Reference Material for quartz was used as the calibration standard.

**2.3.5. Electron paramagnetic resonance (EPR) spectroscopy analysis—**The FSDs and MIN-U-SIL particles were subjected to EPR analysis to determine the presence of silica radicals in the FSDs. EPR measurements were conducted using a Bruker EMX spectrometer (Bruker Instruments Inc.; Billerica, MA) using NMR tubes (Wilmad Glass; Buena, NJ) into which 100 mg of each dry sample was placed. EPR parameters were: center field 3500 ± 100, frequency 9.713 GHz, power 63.3 mW, gain $2.5 \times 10^3$, modulation frequency 100 kHz, modulation amplitude 1.0 G, and time constant 81 ms.

EPR analysis was done using neat FSDs and FSDs that had been subjected to "washing." One gram of FSD was placed in 10 ml of sterile water and the suspension was added to a sterile 75 ml flat-bottomed culture flask and placed on a rocker for 5 d. The sample was then added to a 50 ml culture tube and centrifuged at 2400*g* for 10 min. The supernatant was decanted, and the sample was dried.

**2.3.6. FSD and MIN-U-SIL elemental analysis by ICP—**Elemental analysis of the nine FSDs and MIN-U-SIL using NIOSH Method 7303 (NIOSH Manual of Analytical Methods, 2003) was conducted by BVNA. Table S1 summarizes analyte limits of detection, quantification (LOQ), and analytical range.

## 2.4. Pulmonary inflammatory responses to i.t. instillation of nine FSDs and MIN-U-SIL

The purpose of these experiments was to compare the pulmonary bioactivity of the nine FSDs and MIN-U-SIL.

**2.4.1. Animals—**All studies were conducted in facilities accredited by AAALAC International, were approved by the Institutional Animal Care and Use Committee (approval number 19–010 v4) and were in compliance with the Public Health Service Policy on Humane Care and Use of Laboratory Animals and the NIH Guide for the Care and Use of Laboratory Animals. Male Sprague-Dawley rats ([H1a: (SD) CVF, approximate body weight of 200–275 g at arrival, were obtained from Hilltop Lab Animals, Inc. (Scottdale, PA). All animals were free of viral pathogens, parasites, *Mycoplasma*, *Helicobacter* and cilia-associated respiratory bacillus. Animals were acclimated for one week and housed in pairs in ventilated micro-isolator units supplied with HEPA-filtered laminar flow air (Thoren Caging Systems; Hazleton, PA), with Teklad 7090C Sani Chip and 7070 Diamond Dry combination for bedding, and provided tap water and irradiated Teklad 2918 Global 18% protein rodent chow ad libitum. Rats were housed under controlled light cycle (12 h light/12 h dark) and temperature (22–25 °C) conditions.

### 2.4.2. Treatment of animals with i.t.-administered FSDs and MIN-U-SIL

**2.4.2.1. Sample preparation.:** The FSD and MIN-U-SIL samples were prepared on the day of instillation. Each sample was prepared in a 10 mg/ml stock solution in USP-grade PBS and sonicated for 1 min at ~10 W with a hand-held sonicator to disperse the particles. The high and low doses were prepared by dilution of the stock suspension to 0.5 mg/0.3 ml

PBS and 0.159 mg/0.3 ml PBS, respectively. Each dilution was sonicated for 1 min prior to instillation.

**2.4.2.2. i.t. instillation.:** On day 0, rats were lightly anesthetized with an intraperitoneal injection of 30–40 mg/kg sodium methohexital (PAR Pharmaceutical; Chestnut Ridge, NY). Under anesthesia rats were instilled intratracheally with a low dose (159 μg/rat) or a high dose (500 μg/rat) of each FSD, MIN-U-SIL, or PBS (vehicle control)($n$ = 4 per FSD group and MIN-U-SIL; $n$ = 8 for PBS). All particles were delivered in 0.3 ml of USP-grade PBS. The FSDs were not size-fractionated before-hand but were given as neat materials. The doses were chosen to minimize the possibility of lung particle overload (Borm et al., 2015), and were also based on previous studies in which a 50 μg/rat i.t. administration of MIN-U-SIL did not result in pulmonary effects beyond 1-day post-exposure, but 233 μg/rat caused a variety of inflammatory effects in the lung including increased lung fibrosis in trichrome-stained sections (Farris et al., 2017). To establish the relative toxicities of the FSDs in the present study, 159 μg/rat, which is the half-log interval between 50 and 500 μg/rat, was chosen for use in addition to the 500 μg/rat dose. These doses were well below those (3 mg/rat of quartz as DQ 12) employed by Ernst et al. (2002) and Driscoll et al. (1990a, 1990b) for i.t. administration, but at or below those (500 μg/rat – 5 mg/rat) employed in studies by Sykes et al. (1983). MIN-U-SIL was used as the positive control.

## 2.5. Inflammatory responses: toxicity end points

**2.5.1. Bronchoalveolar lavage (BAL)—**To examine the whether inflammatory responses occurred in the lungs after treatment, rats were exsanguinated following an overdose of sodium pentobarbital euthanasia solution (i.p.; 100–300 mg/kg; Fatal Plus; Vortech Pharmaceuticals) at 30 d post-exposure. The trachea was cannulated, the chest cavity was opened, the left bronchus was clamped off, and BAL was performed on the right lung ($n$ = 4 per group per time point). The first lavage fraction was obtained by filling the right lung with 4 ml of PBS, massaging for 30 s, withdrawing, and repeating the process one more time. This combined aliquot was retained, kept separately, and was designated as the first fraction of BAL fluid (BALF). The following retrieved BALF aliquots were 6 ml in volume, instilled once with light massaging, withdrawn, and combined until a 30 ml volume was obtained. The acellular fluid from the first fraction was retained for further analysis. For each animal, both lavage fractions were centrifuged (10 min, 300 $g$), and the cell pellets were combined and resuspended in 1 ml of PBS.

**2.5.2. BALF analysis: lactate dehydrogenase (LDH) activity—**The presence of LDH activity in the BALF of rats exposed to FSDs, MIN-U-SIL or PBS was measured to evaluate cytotoxicity as an index of lung injury. Measurements of LDH activity in the acellular fluid were obtained using a Cobas C111 analyzer (Roche Diagnostic Systems; Montclair, IN). LDH activity was quantified by detection of the oxidation of lactate coupled to the reduction of $NAD^+$ at 340 nm.

**2.5.3. Cell differentials: alveolar macrophages (AM), neutrophils, lymphocytes and eosinophils—**The total numbers of BAL cells collected from rats treated with FSDs or MIN-U-SIL were counted using a Coulter Multisizer III (Coulter

Electronics; Hialeah, FL). Cell differentials were performed to determine the total number of AM, neutrophils, lymphocytes, and eosinophils. Briefly, $10^5$ cells from each rat were spun down onto slides with a Cytospin 3 centrifuge (Shandon Life Sciences International; Cheshire, England) and labeled with Leukostat stain (Fisher Scientific; Pittsburgh, PA) to differentiate cell types. Two hundred cells per slide were counted, and the percentages of AM, neutrophils, lymphocytes and eosinophils were multiplied by the total number of lavaged cells to calculate the total number of each cell type.

**2.5.4. Lung histopathology—**To provide a visual assessment of the development of lung inflammation, the left lung lobe was pressure-fixed in 10% neutral buffered formalin, embedded, sectioned, and stained with hematoxylin and eosin (H&E). Slides were evaluated for morphologic alterations by a veterinary pathologist, who was blinded to the treatment groups ($n = 4$ per group per time point). Semi-quantitative pathology scores were provided for 1) histiocytic and neutrophilic inflammation in alveoli, 2) alveolar histiocytosis or histiocytic alveolitis, 3) alveolar epithelial cell hypertrophy and hyperplasia, and 4) fibrosis: for severity (0 = none, 1 = minimal, 2 = mild, 3 = moderate, 4 = marked and 5 = severe) and distribution (0 = none, 1 = focal, 2 = locally extensive, 3 = multifocal, 4 = multifocal and coalescent and 5 = diffuse). The pathology score was the sum of the severity and distribution. In this study alveolar histiocytosis was defined as more than three enlarged macrophages per alveolus and/or multiple enlarged macrophages in each of four or more alveoli, excluding alveoli immediately beneath the pleura of the apex of the lung lobe. Histiocytic alveolitis was diagnosed when evidence of inflammation, such as epithelial regeneration or thickening of the alveolar septa, was present in association with a histiocytic macrophage infiltrate. Following the routine evaluation, representative sections of lung from the 500 μg/rat group were examined under polarized light microscopy and the presence of dust particles in macrophages was confirmed.

## 2.6. Statistical analysis

The statistical analysis of the effects of i.t.-administered FSDs and MIN-U-SIL was carried out using JMP v13 for Windows (SAS Institute; Cary, NC). Data were analyzed using analysis of variance, and Dunnett's test to compare each treatment group to the PBS control. Data were also analyzed using the nonparametric equivalent Steel-Dwass test to control family-wise error at 5% in comparing each treatment group to the control. In both cases the overall type I error rate is held to 5% for each variable.

The Mann Whitney $U$ test was used for evaluating semi-quantitative data from the histopathology assessment. Animals were excluded when something other than the test article was identified in the lung as can happen when plant or other material is in the pharynx at the time of intratracheal instillation. A total of 10 rats were removed from the histological analysis for this reason.

For all analyses, significance was set at $P < 0.05$.

# 3. Results

## 3.1. Endotoxin analysis

In order to ascertain whether any biological effects of FSDs could be due to environmental endotoxin contamination, endotoxin levels in the FSDs were analyzed (Table 1). Endotoxin levels above the LOD were detected in every FSD and MIN-U-SIL. The highest level was present in FSD 3 and the lowest level was present in FSD 9. Interestingly, endotoxin was detected in MIN-U-SIL at levels comparable to those found in FSDs. When FSDs or MIN-U-SIL was administered to rats via i.t. instillation, the amount of endotoxin (as EU) in the 0.3 ml of PBS in which the dusts were suspended is insufficient to evoke a biological response. That is, 1 EU = approximately 0.1 ng endotoxin; thus, the highest endotoxin level (FSD 3) is 0.43 ng. The endotoxin analysis performed on one in-house on one sample (FSD 8) was found to be below the limit of detection (<1 EU/mg). In addition, the responses seen in this study are not characteristic of responses to endotoxin and neither endotoxin nor responses to it would be anticipated to persist in the lung at 30 d post-exposure (Rylander and Burrell, 1988; Rylander, 2004).

## 3.2. Physico-chemical characterization of the particles

Upon arrival the FSDs were observed to have different colors, i.e., various degrees of gray or tan, in contrast to MIN-U-SIL, which is white (Fig. 1).

**3.2.1. SEM analysis of FSDs and MIN-U-SIL—**Fig. 2 and Fig. S1 depict SEM images (high and low magnification modes) of neat FSD particles in comparison with MIN-U-SIL. The FSD samples contained angular particles covering a range of sizes, and differences between the FSD particle shapes were unremarkable. Particles as large as 50 μm, and as small as 100 nm, were observed. MIN-U-SIL particles were of more uniform size because they had been sized a priori to be ≤5 μm. For particles of ≤5 μm size there were no obvious differences evident in the shapes of FSD particles compared to MIN-U-SIL particles. In addition, smaller and nanosized particles were adherent to large particles in FSDs and MIN-U-SIL. FSD 9 alone contained numerous spherical particles of varying sizes.

**3.2.2. Dynamic light scattering (DLS)—**DLS was employed to characterize semi-quantitatively the size distributions of the nine FSDs compared to MIN-U-SIL. The results are shown in Fig. 3 and are presented both as intensity and number of particles versus size. This method is not amenable to detection of large particles but did capture distributions of particles of 1100 nm (1.1 μm) or less. The major finding was that the particle size distributions of the dusts were quite different, in terms of both intensity- and number-derived hydrodynamic diameters. The FSD 1, FSD 7 and MIN-U-SIL distributions were mono-modal: those for FSD 1 and FSD 7 reflected the preponderance of particles in the 100 to 700 nm range, while that for MIN-U-SIL spanned 800 to 1300 nm sizes. The other FSDs displayed bi-modal distributions, which were distinct, or which included a larger peak and a shoulder. The peak height for smaller particles was generally at 200 to 300 nm in size. The distributions for FSDs 2, 3, 4 and 5 were comparable. Distributions shapes for density and number, in the context of relative peak heights for small and large particles, were not concordant for many of the FSDs (2, 3, 4, 5, 6, and 8).

### 3.3. Particle characterization: EDS mapping

FSD 8 was used in inhalation experiments described in the tandem papers (Fedan, 2020) and analyzed further here. The results are shown in Fig. 4, Supplementary Figs. S2–S12, and Table 2. MIN-U-SIL consisted entirely of Si and O. Initial analysis of 200 FSD 8 particles, i.e., one location on the particle surface, revealed a mixture of particles of differing elemental compositions that could be categorized into eight groups. The most predominant particles (Group 1) contained Si and O only. The second most common group (Group 2) was comprised of particles containing diverse mixtures of Al, Si, Mg, K, Ca, Mn, Fe, Co, and O. Si, O, and Al were present in the third most common particles (Group 3). Group 4 particles contained Si, O and Fe. Some particles contained no Si and were not abundant. Group 8 particles contained Si, O, Mg and Ca. Thus, nearly half of the particles in FSD were not pure silica, as judged from this level of EDS analysis. Interestingly, Si was not identified in Groups 5 through 7, and all the infrequent particles in these Groups were identified as containing O along with Mg and Ca, Fe, or Fe and S. S was observed in only one instance and was not observed subsequently. It is also important to note that EDX spectra do not discern whether the Si present in samples is in crystalline or amorphous form.

The diversity of the elemental compositions in the Groups prompted the question, are the elements on the surface of a particle of a given group uniformly distributed? To address this question, EDS spectra were obtained from four randomly selected FSD 8 particles of 5–6 μm size, i.e., large enough to locate the EDS detector at several different and distinct regions. Shown in Fig. 5 is the finding that different elements (Fe, K, Al) were detected in different regions of two particles; spectra of two of the other FSD 8 scanned particles revealed only Si and O. Thus, the surface elements on a given particle were heterogeneously distributed.

Following these insights, element mapping of all the FSDs and MIN-U-SIL was then performed to evaluate more completely the elemental distributions on the entire surface of the nine bulk particle samples. Fig. 6 and Supplemental Fig. S13 illustrate that many elements were located on the surfaces of the FSD particles. The spectral fingerprints obtained from the various FSDs were not identical, nor were any of them like MIN-U-SIL's. The composition of each sample was assessed from EDS (Table 4), and it was revealed that the atomic percentages were not uniform among the FSD samples, in agreement with elemental analysis Table 5 (see below). As well, EDS confirmed that MIN-U-SIL did not contain elements (e.g., S, K and Ca) that were present in the FSDs, but did contain Sn, which was not present in the FSDs. Trace levels of thallium (Tl) and silver were observed in FSD 9. These profiles resulting from the mapping of elements indicated that the FSDs from different locales were dissimilar.

Spherical particles of different sizes were observed in SEM views of FSD 9 (Fig. 2 and Fig. S13), but not in the other FSDs. Element mapping of ten random FSD 9 particles with EDS indicated that the elemental fingerprints of all the particles were not identical, especially with respect to the presence of S, Ti and Na. This was reflected in the EDS spectra of the particles and the pseudo-coloration of the particles (Fig. 7).

### 3.4. XRD analysis

The results of the XRD analysis are shown in Table 3. As expected, the FSDs were comprised primarily of α-quartz, the content of which was different in each FSD sample; the highest level was present in FSD 8. Dolomite and tridymite were not detected in any of the FSDs (not shown).

### 3.5. Elemental analysis

The elemental analysis of the nine FSDs and MIN-U-SIL is given in Table 5. The non-silica-elements in greatest abundance (mg/kg; range in parentheses) in FSDs were: Al (330–5400), Ba (12–290), Ca (1200–16,000), Fe (2800–14,000), Mg (160–3900) P (60–440), and K (110–520). MIN-U-SIL contained lesser amounts, but was not devoid of, these elements. In some cases, MIN-U-SIL contained greater amounts of elements (barium, strontium) than some FSDs. FSD 8 had the highest total element content (32,535 mg/kg, 32.5 g/kg, 3.25%) and MIN-U-SIL had the smallest total element content (1438 mg/kg, 1.438 g/kg, 0.14%).

### 3.6. EPR spectroscopy analysis

Fig. 8 illustrates the EPR spectra for the FSDs and MIN-U-SIL. EPR indicated the presence of a strong Si radical signal in MIN-U-SIL. Weak signals were observed for FSDs 1, 2, 3, 5, 6 and 7. The spectrum for FSD 9 was unique. Washing the FSDs had no effect on spectra except in the case of FSD 8, after which a small signal emerged. These findings indicate the presence of impurities and a “masking” of the Si radical in the FSDs, which could be removed partially by washing in the case of FSD 8.

### 3.7. Inflammatory responses: Toxicity end points

Administration of the 159 μg/rat or 500 μg/rat of MIN-U-SIL or the nine FSDs by i.t. instillation had no effect on body weight compared to PBS-treated control animals (Fig. S14).

**3.7.1. Cell differentials: Total BAL cells, AMs, PMNs, lymphocytes and eosinophils—**The total numbers of BAL cells and total PMNs and AMs collected from rats treated with two doses of nine FSDs were unaffected by the FSDs 30 d post-treatment (Fig. 9). MIN-U-SIL, however, elevated significantly the levels of these cells in the BAL in a dose-dependent manner. There were essentially no changes in BAL lymphocytes or eosinophils following administration of the FSDs or MIN-U-SIL (data not shown).

**3.7.2. BALF analysis: LDH activity—**As shown in Fig. 9D, i.t. instillation of the low or high doses of the nine FSDs had no effect on LDH activity in BALF 30 d post-treatment. Whereas instillation of the low dose of MIN-U-SIL increased LDH levels, but not significantly, the high dose of MIN-U-SIL led to a significant increase in LDH levels related to dose.

**3.7.3. Lung histopathology—**Semi-quantitative lung histopathology findings are summarized in Table 6. Examined 30 d post-treatment, foci of histiocytic and neutrophilic alveolitis were present in all three of the rats receiving by i.t. instillation 500 μg of MIN-U-SIL and in two of four rats receiving 159 μg of MIN-U-SIL (Fig. 10). The histiocytic and

neutrophilic alveolitis was accompanied by minimal to mild fibrosis in all three of the rats receiving 500 μg MIN-U-SIL and minimal fibrosis was noted in one of the rats receiving 159 μg MIN-U-SIL. Alveolar epithelial cell hypertrophy and hyperplasia, a classic response to crystalline silica (Miller et al., 1987; Miller and Hook, 1990; Driscoll et al., 1990a; Battelli et al., 2008), was identified in half of the rats receiving 159 μg MIN-U-SIL (Fig. 11). In contrast, histiocytic and neutrophilic alveolitis was limited to one rat in each of four different exposure groups (Fig. S15) among the nine fracking sand dusts (4 of 66 FSD-exposed rats). Fibrosis was identified in 15 of the FSD-exposed rats (6 exposed to 159 μg and 9 exposed to 500 μg). It should be noted that the alveolar septal fibrosis was extremely subtle and unlikely to have been of functional significance.

Small foci of alveolar histiocytosis, small accumulations of alveolar macrophages, were commonly seen in rats exposed to FSD, particularly in rats receiving the 500-μg dose (Fig. 11). FSD particles were sometimes seen in macrophages, indicating the potential to persist in the lung. While the macrophage accumulations were diagnosed as is standard pathology practice (Nikula et al., 2014), half of the concurrent vehicle controls also had small foci of alveolar histiocytosis. This is consistent with the previous reports that alveolar histiocytosis can be seen in normal rats and can also be a normal physiologic and non-adverse response of exposed rats to a particle that will be cleared from the lung or it can be part of an adverse, persistent and/or progressive part of an inflammatory response depending upon severity, the post-exposure time point, and the associated tissue changes (Nikula et al., 2014). In the MIN-U-SIL-exposed rats, neutrophils, a hallmark of overt inflammation, accompanied the histiocytic macrophage response and resulted in the diagnosis of histiocytic and neutrophilic alveolitis noted above. In trichrome-stained sections of lung (Fig. 12), alveolar septa of MIN-U-SIL-treated rats were mildly thickened by blue-staining fibrous connective tissue, indicating mild alveolar septal fibrosis. In addition, a focal foreign body granulomatous response was seen in six of the rats. In four of these rats, elongated fiber-like material sometimes consistent with plant material was associated with this response. This likely represented a response to a few organic dust particles in the workplace FSD, but it is considered distinct from the response to the inorganic FSD. Further, these large particles may not have reached the deep lung when aerosolized. The rats with the foreign body response were, therefore, excluded from the statistical evaluation.

The lungs of both FSD- and MIN-U-SIL-exposed rats had a notable absence of multiple and sometimes coalescing classic silicotic granulomas with prominent collagen fibers (fibrosis) that have been seen in most previous silica instillation studies in rats (Driscoll et al., 1990a; Stettler et al., 1995). This is attributable to the highest dose being below the range where granulomas or significant fibrosis are commonly seen in rats intratracheally exposed to respirable crystalline silica at 28 to 30 d post-exposure (Driscoll et al., 1990b).

## 4. Discussion

In this study the physico-chemical properties and bioactivities of nine FSDs were compared and contrasted with MIN-U-SIL dust, the positive control. In addition, the comparative lung toxicities of these dusts in rats was investigated using i.t. instillations, a screening procedure helpful for initial investigations of comparative pathology (Driscoll et al., 2000). The first

finding of the investigation was that FSDs differed in composition depending on the source of the dusts. This finding is not necessarily surprising, as the proppant sands from which the FSDs arose originated in different geographical regions. The FSDs also differed substantially in their chemical composition compared to MIN-U-SIL. The second finding, i.e., that the each of the FSDs were less toxic to the lung than MIN-U-SIL at the 30-d time point, was unexpected. No obvious differences in toxicity among the FSDs were detected, despite differences in composition among them.

Each of the FSDs contained greater total content of non-silica minerals (0.60–3.25%) compared to MIN-U-SIL (0.14%). Within the FSD category, Al, Ba, Ca, Fe, Mg, P, and K amounts varied considerably among the FSDs, and which one or more of these elements/minerals (or any of the others present) tempered their bioactivity cannot be ascertained from current results. For example, treatment of quartz with soluble aluminum lactate reduces its bioactivity in sheep lungs (Begin et al., 1986, 1987). The capacity of other minerals to produce a similar effect has not been studied. But, clearly, the very low levels of these elements in MIN-U-SIL must contribute to its greater toxicity, perhaps arising from lesser occlusion of particle surfaces by one or more minerals (Harrison et al., 2005).

The sands from which the FSDs arose and the FSDs themselves at mines and at well sites are subjected to many treatments (i.e., washing with water) and environmental influences. It was initially suspected that the endotoxin, a potent inflammatory agent and contaminant of many agents evoking lung diseases, might promote an inflammatory response in the lung after i.t. instillation, and perhaps give rise to larger inflammatory responses than MIN-U-SIL. Therefore, endotoxin levels in FSDs and MIN-U-SIL were measured and found to be quite low. It was noted that endotoxin levels varied among the FSDs. Endotoxin was detected in MIN-U-SIL as well, but its level was lower than that of six of the FSDs, none of which were more bioactive than MIN-U-SIL. Moreover, the ~26-fold difference in endotoxin levels in FSDs 3 and 6 (Table 1) were not manifested in any of the changes in the lung inflammatory parameters. The threshold endotoxin dose in humans and experimental animals is thought to be 5 EU/kg (Malyala and Singh, 2008). The amounts of endotoxin delivered to the rats in association with i.t. administration of the FSDs and MIN-U-SIL ranged from 0.161 to 4.264 EU/kg. These results suggest that neither FSDs nor MIN-U-SIL, at the doses employed, have bioactivity attributable to endotoxin. It is also very unlikely that endotoxin accounts for differences in the bioactivities of FSDs compared to MIN-U-SIL. The FSDs were, in fact, less inflammatory compared to MIN-U-SIL in this assay.

One difference between the nine FSDs and MIN-U-SIL in the lung toxicity study is the FSDs studied were as collected at drilling sites and contained a wide range of particle sizes, including respirable and non-respirable particles, whereas MIN-U-SIL particles were more uniform in size (< 5 μm), respirable, and did not contain large particles such as those contained in the dispersed FSDs. Therefore, the deposition pattern of FSDs following instillation may have differed from that of MIN-U-SIL. The larger particles in the FSDs will not have permeated the smaller airways as effectively as the ones around the respirable range. Inasmuch as the doses given to the animals were weight-based, the presence of large particles in the neat FSDs could have led to a seeming reduction in toxicity that would otherwise have occurred had the instilled FSD samples contained only particles the same

size as MIN-U-SIL, everything else being the same. This may have contributed to the greater alveolar toxicity of MIN-U-SIL compared to the FSDs in this study. However, other evidence suggests that this does not fully explain the relatively lower toxicity of FSDs compared with MIN-U-SIL. In inhalation studies, after 90 d post-exposure FSD 8 did not give rise to the pro-fibrogenic response characteristic of that evoked by MIN-U-SIL (Sager et al., 2020), i.e., under conditions which establish a pro-fibrotic response to inhaled MIN-U-SIL, inhalation of smaller, more uniform FSD 8 particles (mass median aerodynamic particle diameter ~ 1.75 μm) also did not evoke a similar response. Although size difference was less than for the other FSDs, the total non-silica element content of FSD 8 was the most of any FSD and may have contributed to differences from MIN-U-SIL. Inhalation exposures with size-fractionated, respirable FSDs can be used in future experiments to compare directly the toxicities of MIN-U-SIL *vis à vis* FSDs on indices of pulmonary inflammation.

A number of studies (Begin et al., 1986, 1987; Donaldson et al., 2001) have reported that coating of silica particles with aluminum lactate (and other agents) reduces the pulmonary response to crystalline silica. The aluminum in FSDs may have exerted this effect. Having said this, the aluminum content of FSD 7 was less than that of MIN-U-SIL, indicating that, by itself, aluminum cannot account for the differences in the bioactivities of all the FSDs compared to MIN-U-SIL. The effects of “coating” crystalline silica with the other elements found in the FSDs has not been well characterized, nor have they been evaluated for their ability, alone or in concert with aluminum, to reduce lung toxicity. Donaldson et al. (2001) have advanced a similar idea, noting that coating of quartz particle surfaces by minerals or coal mine dusts affects the bioactivity of the particles.

In studies (Chen et al., 2005; Harrison et al., 2005) in which toxicities of silica dusts among tin and tungsten mine and pottery workplaces were compared, lung toxicity was found to be related to the extent of “occlusion” of particle surfaces by alumino-silicate. That is, greater occlusion reducing the amount of available crystalline silica at the particle surface, at which interactions with inflammatory cells occurs, led to reduced toxicity. The present study supports this conclusion in three ways: first, EDS analysis of FSD 8 indicated that there are places on particle surfaces which reveal the presence of silica alone, and other locations where silica is found in association with potassium, aluminum, and/or iron, indicating surfaces of FSD are not homogeneous with respect to element distribution. Second, the presence of areas of surface lacking or containing other elements in association with silica is a correlate to the surface “occlusion” idea proposed by Chen et al. (2005) and Harrison et al. (2005) as a potential factor in reducing the relative toxicity of some silica-containing dusts. Third, the presence of the minerals on the silica particle surface potentially blunts toxicity in the lung, which can tentatively be ascribed to surface occlusion.

Whereas the FSDs are essentially crystalline silica materials containing impurities and coatings, EPR analysis revealed similar spectra for these dusts that collectively differed from that of MIN-U-SIL in that they did not reveal a strong Si radical signal. It was suspected that the Si radical signal was masked by impurities in the dusts. Following extensive washing of the FSDs in water, the spectra were not changed except in the case of FSD 8, for which a small Si radical signal emerged. The identity of the material(s) producing this masking effect is unknown, but it is assumed that it is associated with one or more minerals contained in the

FSDs. This is consistent with a previous study demonstrating that HCl-washed silica produced much greater changes in alveolar phospholipids than unwashed silica in rats (Miles et al., 1994), and raises the possibility that the bioactivity of FSD 8 could result from particle effects as well as extractable agent effects. This latter concept was explored in Olgun et al. (2020).

A major purpose of this investigation was to obtain information about the relative toxicogenic activities of the nine FSDs to establish similarities and differences to one, i.e., FSD 8, that was investigated in more detail following inhalation exposure (see Fedan, 2020). A direct comparison was made between the effects of i.t.-administered FSDs and MIN-U-SIL. At this time point, MIN-U-SIL, but not the FSDs, initiated inflammatory responses in the manner reported in the rat after inhalation (Porter et al., 2001). MIN-U-SIL administration induced dose-dependent increases in multiple inflammatory markers: total BAL cells, total BAL PMNs, LDH activity and total BAL alveolar macrophages. These changes were not observed in rats treated with any of the FSDs. The histopathological findings were in agreement with these results and revealed appreciable differences in the degrees to which MIN-U-SIL and the FSDs collectively evoked histiocytic and neutrophilic inflammation and fibrosis in the lungs of treated animals, with MIN-U-SIL treatment leading to robust responses and the FSDs muted or undetectable responses.

It is reasonable to conclude that the lack of pro-inflammatory bioactivity of the FSDs in the lung at this time point in comparison to MIN-U-SIL is related to the presence of minerals in the FSDs. These minerals may have altered the surface reactivity, reduced cytotoxicity, and/or facilitated pulmonary clearance relative to MIN-U-SIL at this time point. However, limitations of this i.t. instillation study are the single post-exposure time point and particle size differences between the FSDs and MIN-U-SIL that may have affected deposited particle surface area on a mass basis. Further research could consider comparing the toxicological effects of FSDs vs. washed FSDs, the bioactivity of the materials that can be extracted from the dusts, and the effects of a broader range of exposure doses and time points, and comparisons between inhalable fractions of the dusts, to understand the basis of the apparently muted effects of FSDs in the lungs of i.t.-instilled animals under conditions of this study. In short, recognizing that dusts containing crystalline silica are responsible for severe lung disease in workers (National Institute for Occupational Safety and Health (NIOSH), 2002a, 2002b; Silicosis and Silicate Disease Committee, 1988), it is important to investigate factors that make some silica-containing dusts more hazardous than others (Cohen et al., 2016; National Institute for Occupational Safety and Health (NIOSH), 2002a, 2002b; Silicosis and Silicate Disease Committee, 1988). What this intratracheal instillation study clearly showed was that at this time point and at these doses, the biological effects of these different FSDs had many similarities.

In the papers that follow this one, the biological effects of FSD exposure in several organ systems following inhalation will be described. In the lung several observations will be presented which indicate that the effects of FSD 8 are different from those reported in animal models of silicosis induced with MIN-U-SIL. The effects of FSD exposure on other organ systems, not heretofore described, also are reported.

## Supplementary Material

Refer to Web version on PubMed Central for supplementary material.

## Acknowledgements

Funding was provided by the National Institute for Occupational Safety and Health, Project Number 7927ZLDC. Assistance with organizing and analyzing semi-quantitative histopathology data was provided by Sidney Clingerman and Samantha Service.

## References

Anderson SE, Shane H, Long C, Marrocco A, Lukomska E, Roberts JR, Marshall N, Fedan JS, 2020 Biological effects of inhaled hydraulic fracturing sand dust. VIII. Immunotoxicity. Toxicol. Appl. Pharmacol 408, 115256 10.1016/j.taap.2020.115256. [PubMed: 33007384]

Battelli LA, Ghanem MM, Kashon ML, Barger M, Ma JY, Simoskevitz RL, Miles PR, Hubbs AF, 2008 Crystalline silica is a negative modifier of pulmonary cytochrome P-4501A1 induction. J. Toxicol. Environ. Health A 71, 521–532. [PubMed: 18338287]

Begin R, Masse S, Rola-Pleszczynski M, Martel M, Desmarais Y, Geoffroy M, LeBouffant L, Daniel H, Martin J, 1986 Aluminum lactate treatment alters the lung biological activity of quartz. Exp. Lung Res 10, 385–399. [PubMed: 3013607]

Begin R, Masse S, Sebastien P, Martel M, Bosse J, Dubois F, Geoffroy M, Labbe J, 1987 Sustained efficacy of aluminum to reduce quartz toxicity in the lung. Exp. Lung Res 13, 205–222. [PubMed: 2822380]

Borm P, Cassee FR, Oberdörster G, 2015 Lung particle overload: old school -new insights? Part. Fibre Toxicol 12, 10. [PubMed: 25927223]

Castranova V, Dalal NS, Vallyathan V, in Castranova V, Vallyathan, Wallace WE (Eds.), 1996 Silica and Silica-Induced Lung Diseases. CRC Press, Boca Raton, FL.

Castranova V, Porter D, Millecchia L, Ma JY, Hubbs AF, Teass A, 2002 Effect of inhaled crystalline silica in a rat model: time course of pulmonary reactions. Mol. Cell. Biochem 234–235, 177–184.

Chen W, Hnizdo E, Chen JQ, Attfield MD, Gao P, Hearl F, Lu J, Wallace WE, 2005 Risk of silicosis in cohorts of Chinese tin and tungsten miners, and pottery workers (I): an epidemiological study. Am. J. Ind. Med 48, 1–9. [PubMed: 15940718]

Cohen RA, Petsonk EL, Rose C, Young B, Regier M, Najmuddin A, Abraham JL, Churg A, Green FH, 2016 Lung pathology in U.S. coal workers with rapidly progressive pneumoconiosis implicates silica and silicates. Am. J. Respir. Crit. Care Med 193, 673–680. [PubMed: 26513613]

Department of Health and Human Services, Centers for Disease Control and Prevention, National Institute for Occupational Safety and Health, Vol. DHHS (NIOSH) Publication No. 2002-129.

Donaldson K, Stone SV, Duffin R, Cloutier A, Schins R, Borm P, 2001 The quartz hazard: effects of surface matrix on inflammagenic activity. J. Environ. Pathol. Toxicol. Oncol 20 (Supple 1), 109–118.

Driscoll KE, Lindenschmidt RC, Maurer JK, Higgins JM, Ridder G, 1990a Pulmonary response to silica or titanium dioxide: inflammatory cells, alveolar macrophage-derived cytokines, and histopathology. Am. J. Respir. Cell Mol. Biol 2, 381–390. [PubMed: 2157474]

Driscoll KE, Maurer JK, Lindenschmidt RC, Romberger D, Rennard SI, Crosby L, 1990b Respiratory tract responses to dust: relationships between dust burden, lung injury, alveolar macrophage fibronectin release, and the development of pulmonary fibrosis. Toxicol. Appl. Pharmacol 106, 88–101. [PubMed: 2174581]

Driscoll KE, Costa DL, Hatch G, Henderson R, Oberdörster G, Salem H, Schlesinger RB, 2000 Intratracheal instillation as an exposure technique for the evaluation of respiratory tract toxicity: uses and limitations. Toxicol. Sci 55, 24–35. [PubMed: 10788556]

Ernst H, Rittinghausen S, Bartsch W, Creutzenberg O, Dasenbrock C, Görlitz BD, Hecht M, Kairies U, Muhle H, Müller M, Heinrich U, Pott F, 2002 The acquisition of multidimensional NMR spectra within a single scan. Proceeding of the national academy of science 54, 109–126.

Esswein EJ, Breitenstein M, Snawder J, Kiefer M, Sieber WK, 2013 Occupational exposures to respirable crystalline silica during hydraulic fracturing. J. Occup. Environ. Hyg 10, 347–356. [PubMed: 23679563]

Leung CC, Yu ITS, Chen W, 2012 Silicosis. Lancet 379, 2008–2018. [PubMed: 22534002]

Farris BY, Antonini JM, Fedan JS, Mercer RR, Roach KA, Chen BT, Schwegler-Berry D, Kashon ML, Barger MW, Roberts JR, 2017 Pulmonary toxicity following acute coexposures to diesel particulate matter and α-quartz crystalline silica in the Sprague-Dawley rat. Inhal. Toxicol 29 (7), 322–339. [PubMed: 28967277]

Fedan JS, 2020 Biological effects of inhaled hydraulic fracturing sand dust. I. Scope of the investigation. Toxicol. Appl. Pharmacol (Manuscript submitted to this journal as a tandem paper to accompany this manuscript).

Harrison J, Chen JQ, Miller W, Chen W, Hnizdo E, Lu J, Chisholm W, Keane M, Gao P, Wallace W, 2005 Risk of silicosis in cohorts of Chinese tin and tungsten miners and pottery workers (II): workplace-specific silica particle surface composition. Am. J. Ind. Med 48, 10–15. [PubMed: 15940714]

Krajnak K, Russ KA, McKinney W, Waugh S, Zheng W, Kan H, Kashon ML, Johnson C, Cumpston J, Fedan JS, 2020 Biological effects of inhaled hydraulic fracturing sand dust. IV. Cardiovascular effects. Toxicol. Appl. Pharmacol, 115242 10.1016/j.taap.2020.115242. [PubMed: 32931794]

Silicosis and Silicate Disease Committee, 1988 Diseases associated with exposure to silica and nonfibrous silicate minerals. Arch. Pathol. Lab. Med 112, 673–720. [PubMed: 2838005]

Sriram K, Lin GX, Jefferson AM, McKinney W, Jackson MC, Cumpston A, Cumpston JL, Cumpston JB, Leonard HD, Kashon ML, and Fedan JS, 2020 Biological effects of inhaled hydraulic fracturing sand dust. VII. Neuroinflammation and altered synaptic protein expression. Toxicol. Appl. Pharmacol (manuscript submitted to this journal as a tandem paper to accompany this manuscript.).

Malyala P, Singh M, 2008 Tndotoxin limits in formulations for pre-clinical research. J. Pharm. Sci 97, 2041–2044. [PubMed: 17847072]

McDonald JC, McDonald AD, Hughes JM, Rando RJ, Weill H, 2005 Mortality from lung and kidney disease in a cohort of north American industrial sand workers: an update. Ann. Occup. Hyg 49, 367–373. [PubMed: 15728107]

Miles PR, Bowman L, Jones WG, Berry DS, Vallyathan V, 1994 Changes in alveolar lavage materials and lung microsomal xenobiotic metabolism following exposures to HCl-washed or unwashed crystalline silica. Toxicol. Appl. Pharmacol 129, 235–242. [PubMed: 7992313]

Miller BE, Hook GE, 1990 Hypertrophy and hyperplasia of alveolar type II cells in response to silica and other pulmonary toxicants. Environ. Health Perspect 85, 15–23. [PubMed: 2166657]

Miller BE, Dethloff LA, Gladen BC, Hook GE, 1987 Progression of type II cell hypertrophy and hyperplasia during silica-induced pulmonary inflammation. Lab. Investig 57, 546–554. [PubMed: 2824924]

National Institute for Occupational Safety and Health (NIOSH), 2002a Health Effects of Occupational Exposure to Respirable Crystalline Silica, DHHS (NIOSH) Publication No. 2002–1292002 https://www.cdc.gov/niosh/docs/2002-129/pdfs/2002-129.pdf?id=10.26616/NIOSHPUB2002129.

National Institute for Occupational Safety and Health (NIOSH), 2002b NIOSH Manual of Analytical Methods, 4th edition https://www.cdc.gov/niosh/docs/2003-154/default.html.

Nikula KJ, McCartney JE, McGovern T, Miller GK, Odin M, Pino MV, Reed MD, 2014 STP position paper: interpreting the significance of increased alveolar macrophages in rodents following inhalation of pharmaceutical materials. Toxicol. Pathol 42, 472–486. [PubMed: 24178583]

Olgun NS, Morris AM, Stefaniak AB, Bowers LN, Knepp AK, Duling MG, Mercer RR, Kashon ML, Fedan JS, Leonard SS, 2020 Biological effects of inhaled hydraulic fracturing sand dust. III. Cytotoxicity and pro-inflammatory responses in cultured murine macrophage cells. Toxicol. Appl. Pharmacol 408, 115281 10.1016/j.taap.2020.115281. [PubMed: 33065155]

Porter DW, Ramsey D, Hubbs AF, Battelli L, Ma J, Barger M, Landsittel D, Robinson VA, McLaurin J, Khan A, Jones W, Teass A, Castranova V, 2001 Time course of pulmonary response of rats to inhalation of crystalline silica: histological results and biochemical indices of damage, lipidosis, and fibrosis. J. Environ. Pathol. Toxicol. Oncol 20 (Suppl. 1), 1–14.

Porter DW, Ye J, Ma J, Barger M, Robinson VA, Ramsey D, McLaurin J, Khan A, Landsittel D, Teass A, Castranova V, 2002 Time course of pulmonary response of rats to inhalation of crystalline silica: NF-kappa B activation, inflammation, cytokine production, and damage. Inhal. Toxicol 14, 349–367. [PubMed: 12028809]

Porter DW, Hubbs AF, Mercer R, Robinson VA, Ramsey D, McLaurin J, Khan A, Battelli L, Brumbaugh K, Teass A, Castranova V, 2004 Progression of lung inflammation and damage in rats after cessation of silica inhalation. Toxicol. Sci 79, 370–380. [PubMed: 15056817]

Russ KA, Thompson JA, Reynolds JS, Mercer RR, Porter DW, McKinney W, Dey RD, Barger M, Cumpston J, Batchelor TP, Kashon ML, Kodali V, Sriram K, Fedan JS, 2020 Biological effects of inhaled hydraulic fracturing sand dust. IV. Pulmonary effects. Toxicol. Appl. Pharmacol, 115284 10.1016/j.taap.2020.115284m. [PubMed: 33068619]

Rylander R, 2004 Organic dusts and disease: a continuous research challenge. Am. J. Ind. Med 46, 323–326.

Rylander R, Burrell R, 1988 Endotoxins in inhalation research. Summary of conclusions of a workshop held at Clearwater, Florida, U.S.A., 28–30 September 1987. Ann. Occup. Hyg 32, 553–556. [PubMed: 3228266]

Sager TM, Roberts JR, Umbright CM, Barger M, Kashon ML, Fedan JS, Joseph P, 2020 Biological effects of inhaled hydraulic fracturing sand dust. V. Pulmonary inflammatory, cytotoxic and oxidant effects. Toxicol. Appl. Pharmacol, 115280 10.1016/j.taap.2020.115280 (manuscript submitted to this journal as a tandem paper to accompany this manuscript.). [PubMed: 33065154]

Stettler LE, Salomon RA, Platek SF, Moorman WJ, Clark JC, Krieg EF, Phipps FC, 1995 Fibrogenic potentials of coal slags used as abrasive blasting substitutes. J. Toxicol. Environ. Health 45, 349–365. [PubMed: 7609007]

Sykes SE, Morgan A, Moores A, Jones ST, Holmes A, Davison W, 1983 Evidence for a dose-dependent inflammatory response to quartz in the rat lung and its significance in early changes in collagen metabolism. Environ. Health Perspect 51, 141–146. [PubMed: 6315354]

Investigative Team, 2020 Biological effects of inhaled hydraulic fracturing sand dust. IX. Summary and significance. Toxicol. Appl. Pharmacol 18.

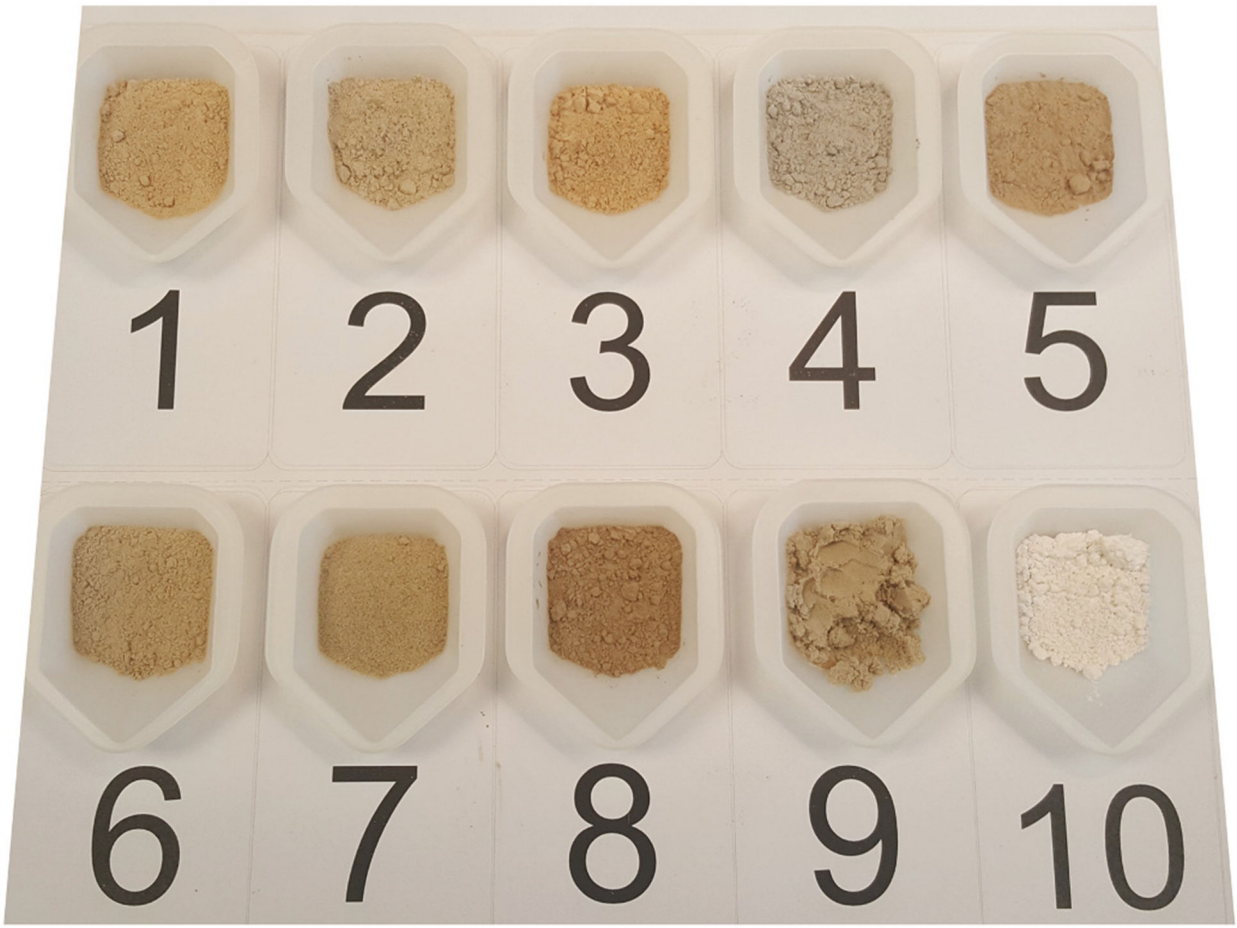


**Fig. 1.**
Photograph of the nine FSDs studied in this investigation. These FSDs were collected at sites (see 2.1.) where hydraulic fracturing was used. The FSDs exhibited a range of colors. MIN-U-SIL (number 10) is included for comparison.

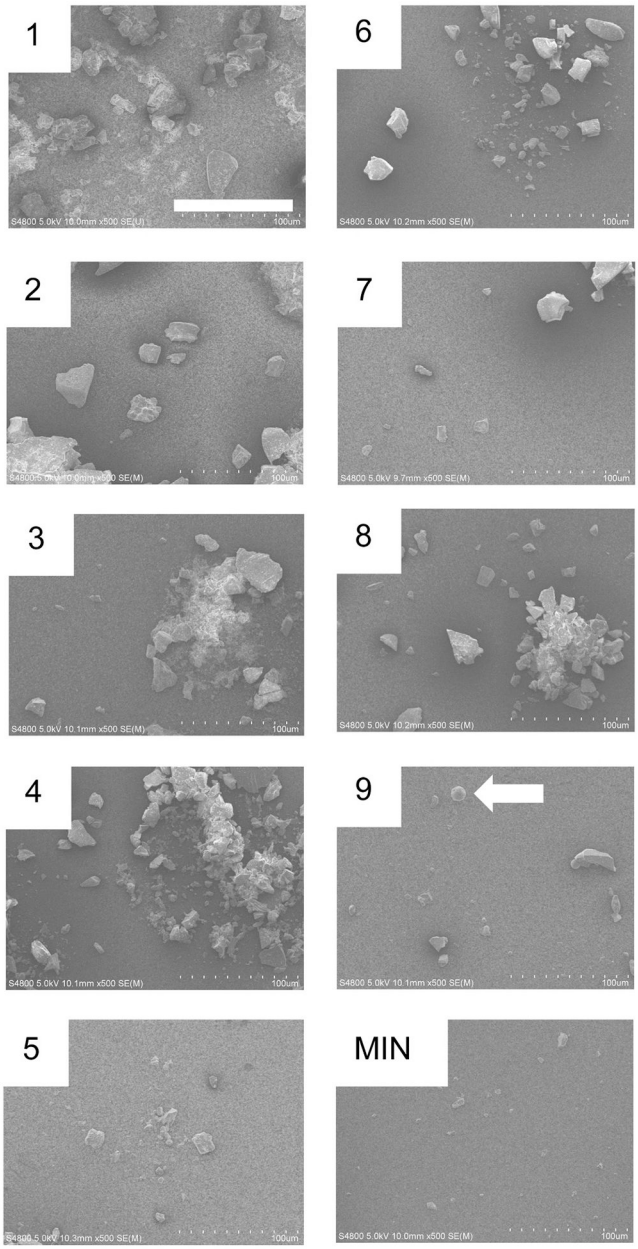


**Fig. 2.**

High magnification SEM images of the nine FSDs studied in this investigation. MIN-U-SIL (MIN) is shown for comparison. Bar = 100 μm. Note the spherical structures in FSD 9 (arrow). Refer to Fig. S1 for a lower power rendering of the FSDs.

High magnification SEM images of the nine FSDs studied in this investigation. MIN-U-SIL (MIN) is shown for comparison. Bar = 100 μm. Note the spherical structures in FSD 9 (arrow). Refer to Fig. S1 for a lower power rendering of the FSDs.

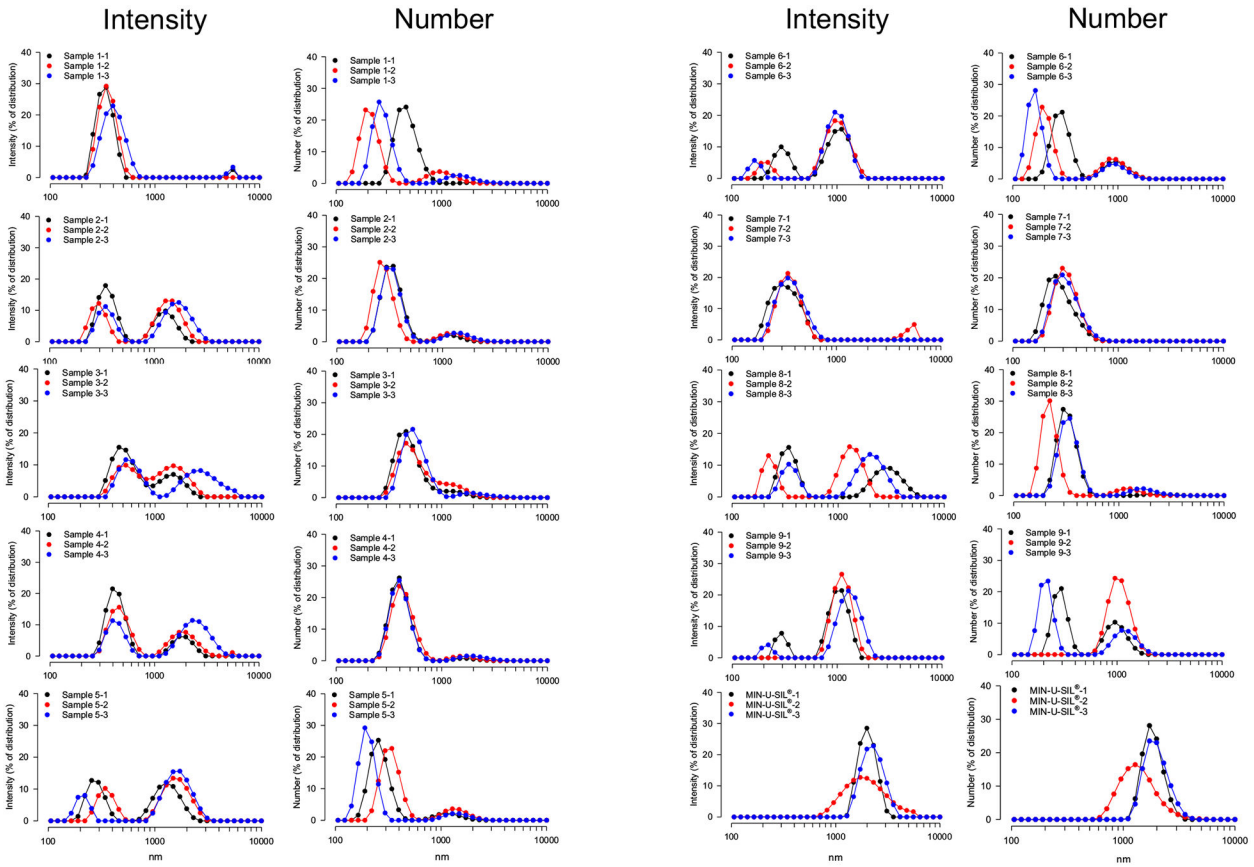


**Fig. 3.**

DLS intensity and particle size distributions of nine FSDs and MIN-U-SIL. The black, red and blue colors refer to three separate measurements on a given sample.

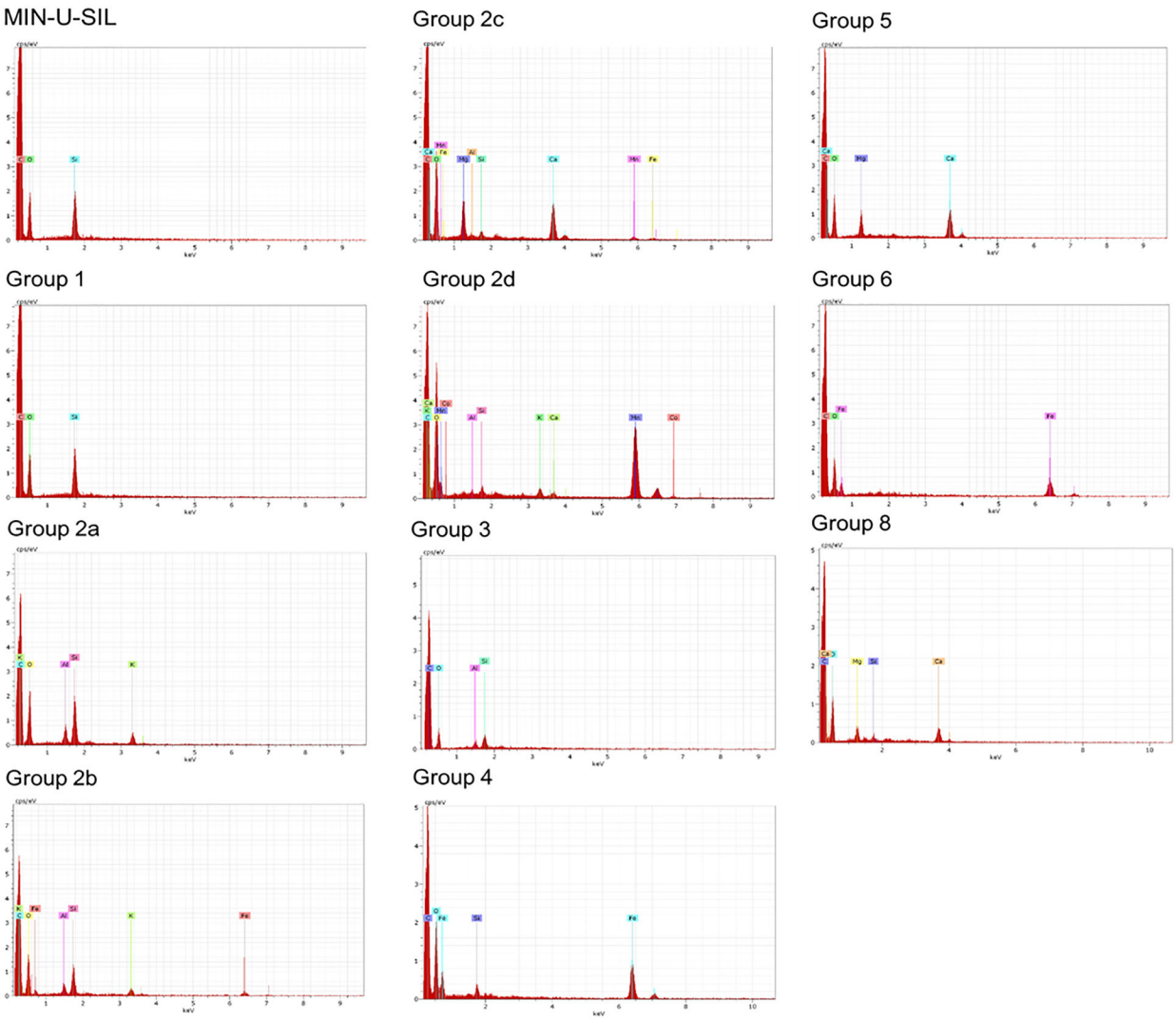


**Fig. 4.**

EDS spectrum analysis of MIN-U-SIL and FSD 8. Eight distinct groups of particles based on surface element content were detected. These spectra are representative of ones detected in a survey of 200 FSD 8 particles. For each particle, a spectrum was obtained from one discrete spot on the particle surface. Abscissa: keV; ordinate: cps/eV. The individual spectra are also presented as Supplementary Figs. S2–S12 for greater clarity, along with SEM images identifying beam location. EDS spectrum analysis of MIN-U-SIL and FSD 8. Eight distinct groups of particles based on surface element content were detected. These spectra are representative of ones detected in a survey of 200 FSD 8 particles. For each particle, a spectrum was obtained from one discrete spot on the particle surface. Abscissa: keV; ordinate: cps/eV. The individual spectra are also presented as Supplementary Figs. S2–S12 for greater clarity, along with SEM images identifying beam location.

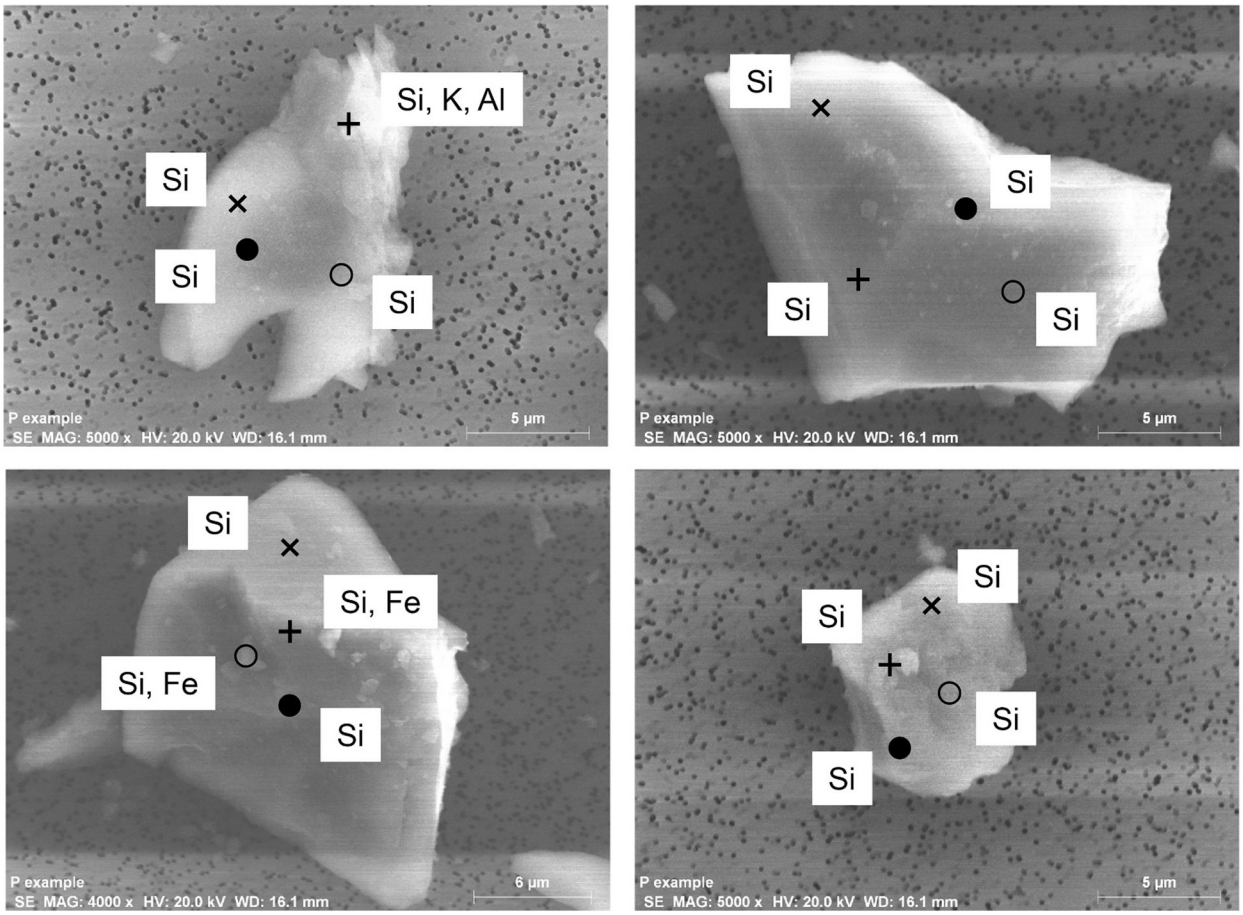


**Fig. 5.**

EDS analysis of the surface of randomly selected FSD particles, indicating heterogeneity of surface elemental composition on single particles (upper and lower left) or absence of elements other than Si in areas scanned in other particles (upper and lower right). The symbols indicate the several locations of the electron beam at on the particles, and the elements identified at each location are shown.

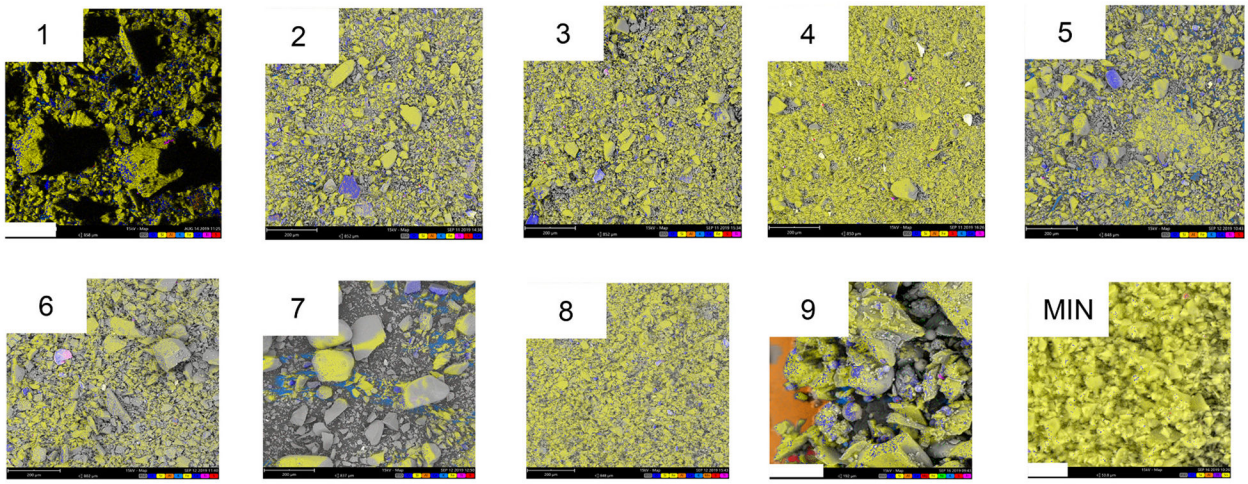


**Fig. 6.**

Composite EDS images of nine neat FSDs and MIN-U-SIL. These images depict the composite pseudo-colors of the samples. With amplification of the images different colors appear more clearly, reflecting the location of elements at different locations on the particles. For FSD 9 the orange area reflects the Al present in the mounting stub on which the particles were placed for analysis. The spectra for the individual elements comprising the composite in these samples may be viewed in Fig. S13.

Composite EDS images of nine neat FSDs and MIN-U-SIL. These images depict the composite pseudo-colors of the samples. With amplification of the images different colors appear more clearly, reflecting the location of elements at different locations on the particles. For FSD 9 the orange area reflects the Al present in the mounting stub on which the particles were placed for analysis. The spectra for the individual elements comprising the composite in these samples may be viewed in Fig. S13.

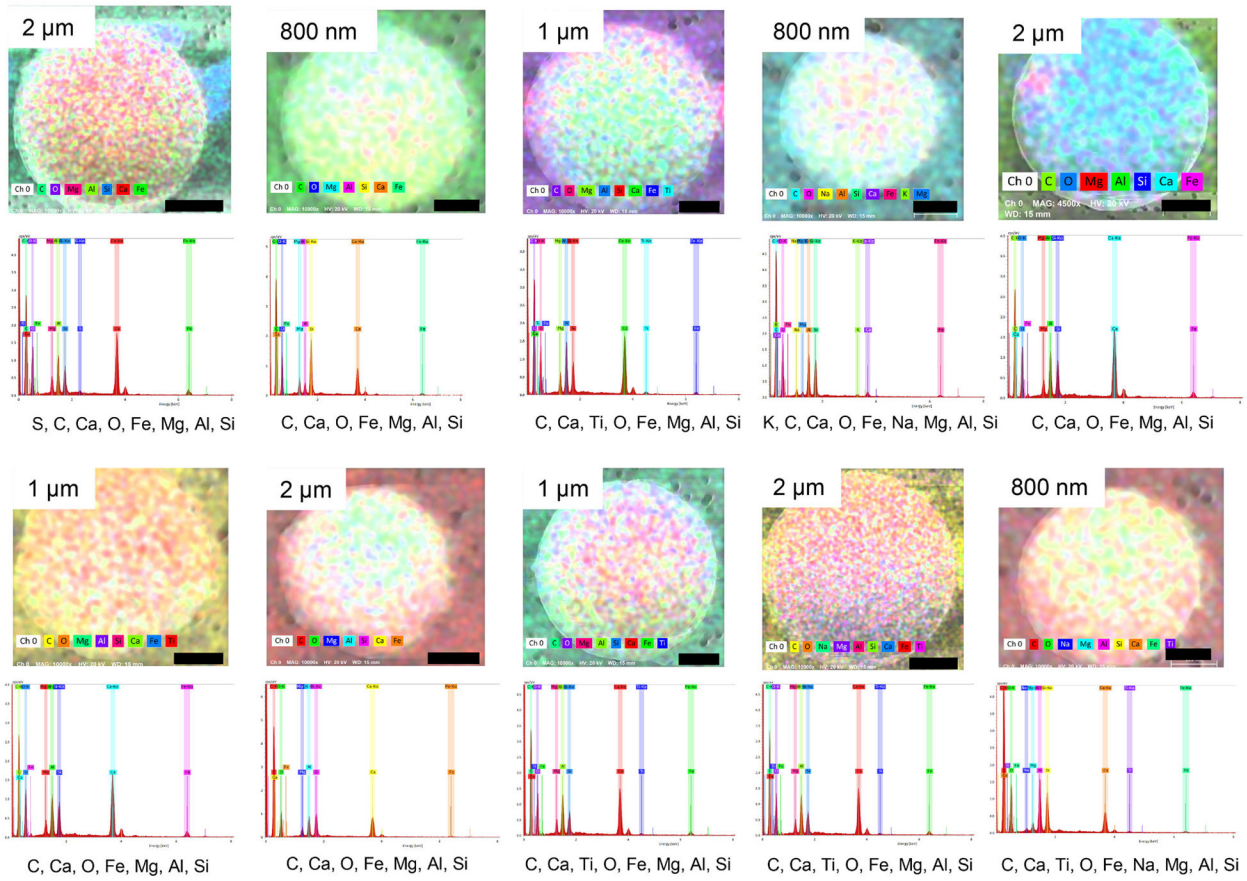


**Fig. 7.**

Composite EDS images of spherical structures found in FSD 9. Spheres of different sizes were observed in the neat sample. The EDS spectrum of each sample is shown below its composite image. These images depict the composite pseudo-colors of the samples. In this figure the composite pseudo-color reflects the predominance of the elements; the instrument assigns color with regard to predominance as opposed to assigning a given color with a given element, as was done in Fig. 6. With augmentation of the images different colors appear more clearly, reflecting the location of elements at different locations. The rank order of element prevalence is shown by the order of the elements below each panel, from left to right. The dimensions of the black bars are given by the insets in the upper left-hand corner of each panel.

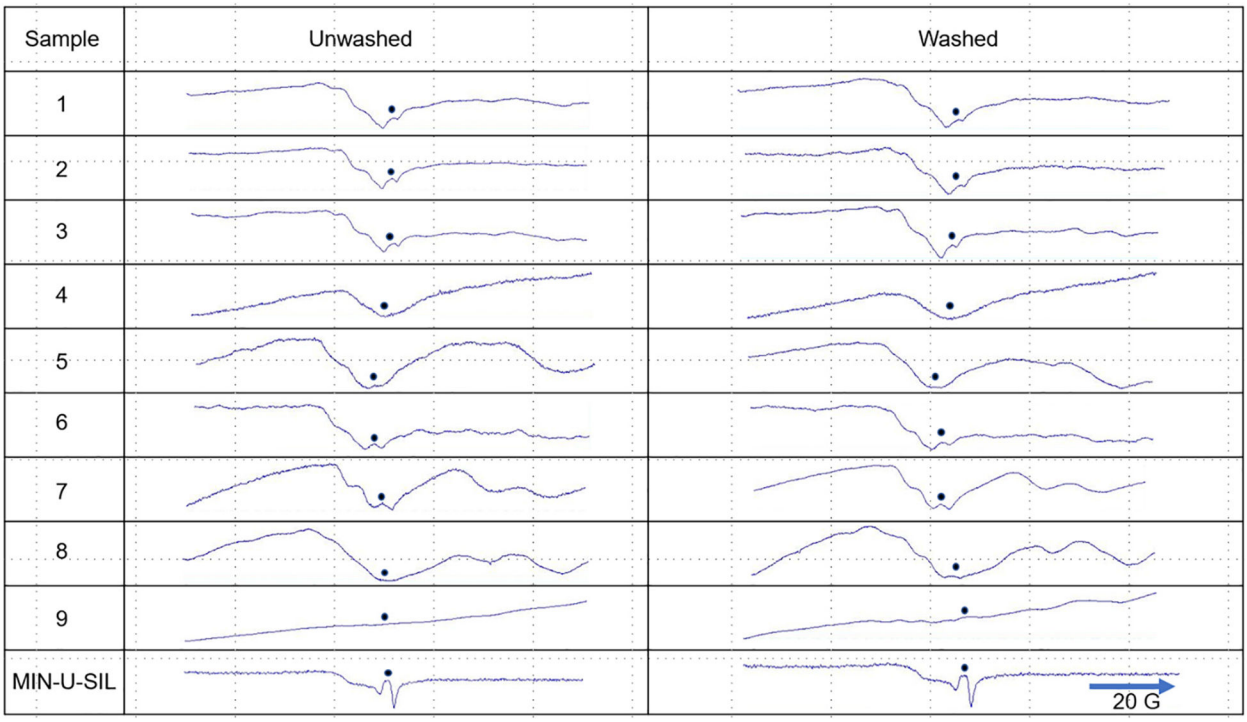


**Fig. 8.**

EPR spectra of nine neat FSDs before (left column) and after (right column) washing in $dH_2O$. The dots indicate the location of the visible or masked Si radical signal in the spectra. Only in the case of FSD 8 did washing partially revert the Si signal to that of MIN-U-SIL. See also Castranova et al. (1996) for EPR spectra of MIN-U-SIL.

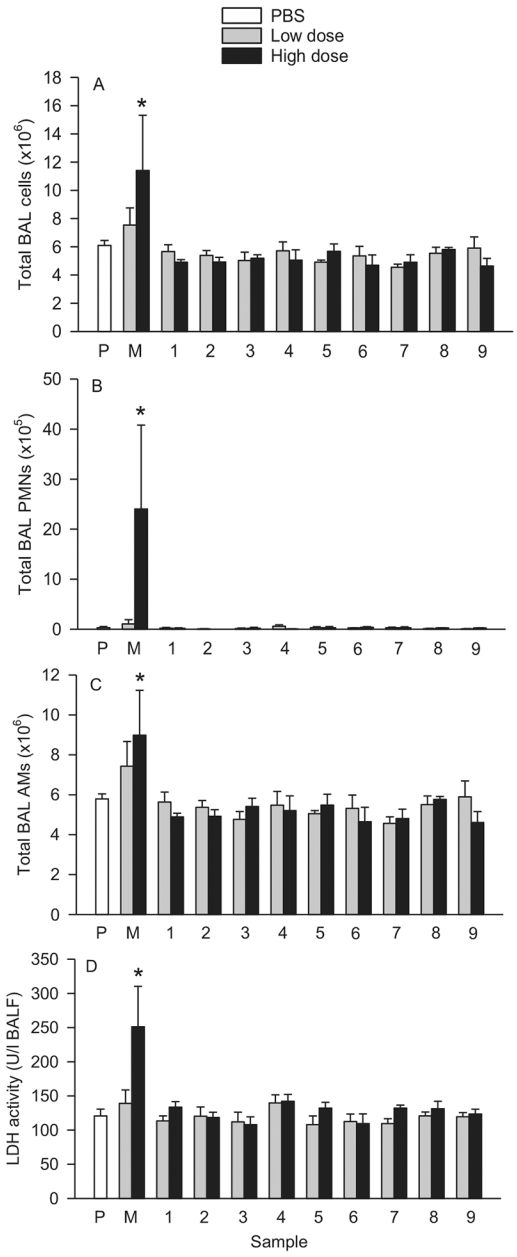


**Fig. 9.**

Effects of nine neat FSDs and MIN-U-SIL (M) on BAL inflammatory cellular and LDH responses following i.t. instillation of the dusts in rats. A, Total BAL cells; B, total BAL PMNs; C, total BAL AMs; and D, LDH activity. The dusts were administered in a low dose (159 μg/rat) or a high dose (500 μg/rat). Cell and LDH activity measurements were obtained from BAL 30 d post-instillation exposure. *Significantly different from PBS (P). $n = 4$.

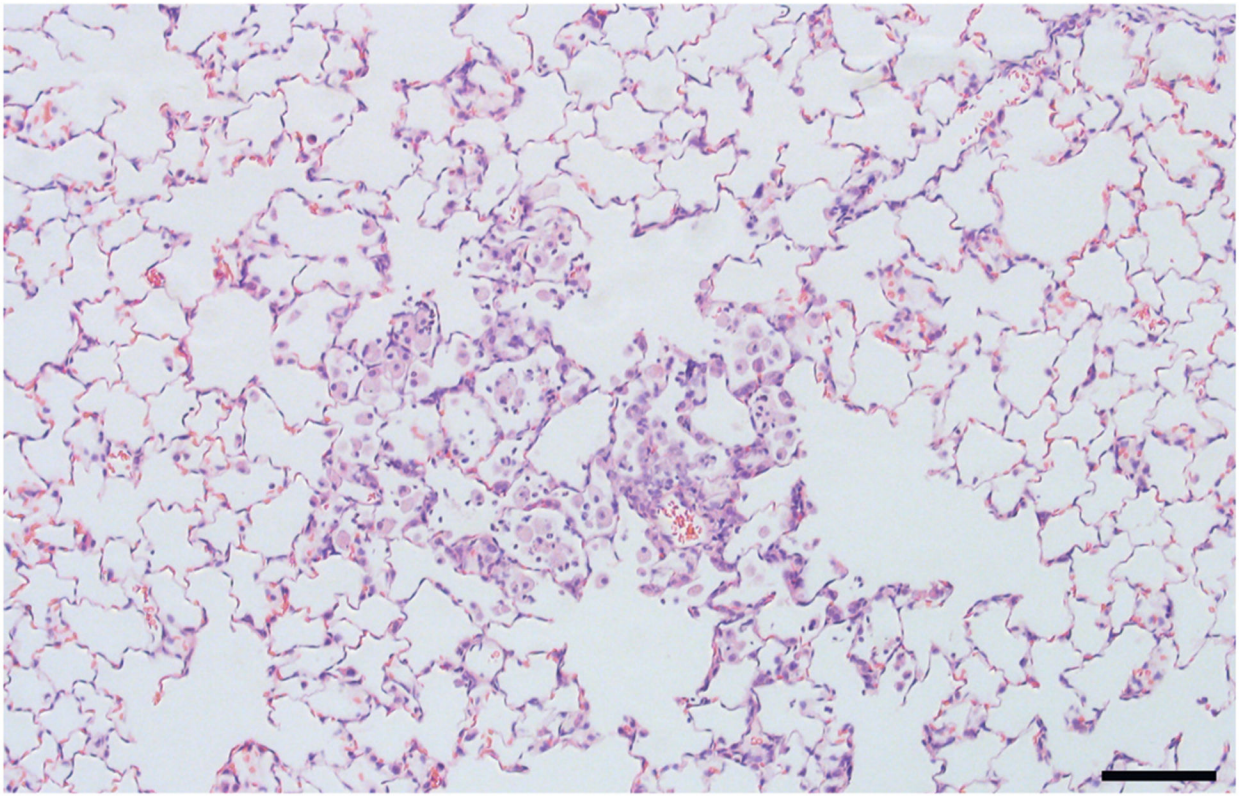

**Fig. 10.**

A focus of histiocytic and neutrophilic alveolitis in a rat exposed to 500 μg MIN-U-SIL by i.t. instillation 30 d earlier. Bar = 100 μm.

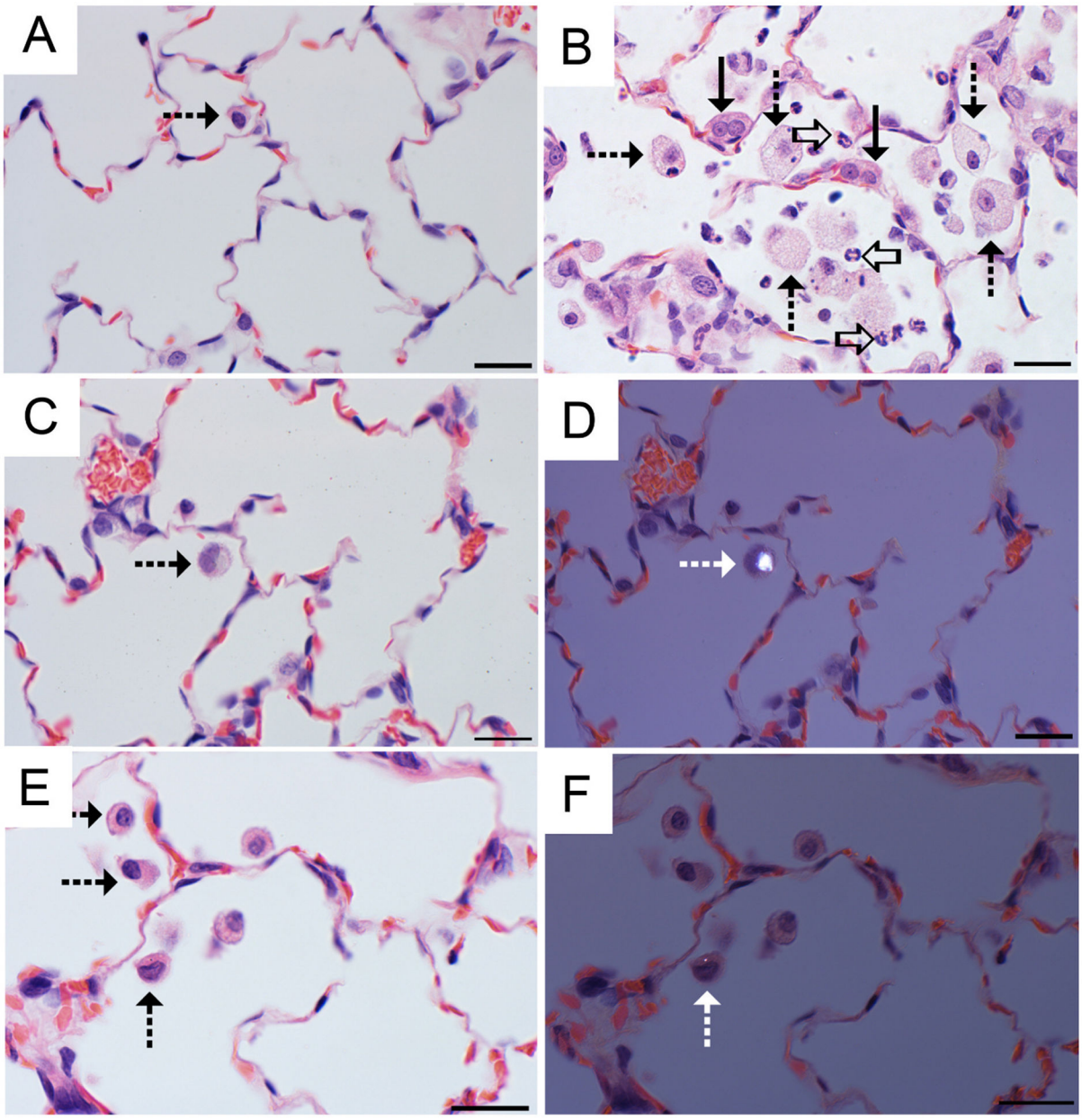


**Fig. 11.**

Foci of histiocytic and neutrophilic alveolitis characterized the response to the 500 μg MIN-U-SIL dose but was rarely observed in FSD-exposed rats. Alveolar macrophages containing FSD particles were occasionally observed in the 500 μg FSD-exposed rats. A, Alveolar region of a vehicle control (PBS). The alveolar macrophage (dashed arrow) is a normal feature. B, Histiocytic and neutrophilic alveolitis 30 d after a 500 μg MIN-U-SIL exposure is characterized by increased number and size of alveolar macrophages (dashed arrows) accompanied by neutrophils (open arrows). Alveolar epithelial cells are increased in number and size, reflecting hyperplasia and hypertrophy (solid arrows). C, Lung of a rat 30 d after receiving a 500 μg FSD 8. An occasional macrophage (dashed arrows) is in the alveolar region. D, Polarized image from the same field shown in C, demonstrating a birefringent

particle. E, Lung of a rat 30 d after receiving a 500 μg FSD 5. Low numbers of alveolar macrophages (dashed arrows) are seen in the alveolar region. F, Polarized image from the same field shown in E, demonstrating a birefringent particle in one of the alveolar macrophages. H and E stain; bar = 20 μm.

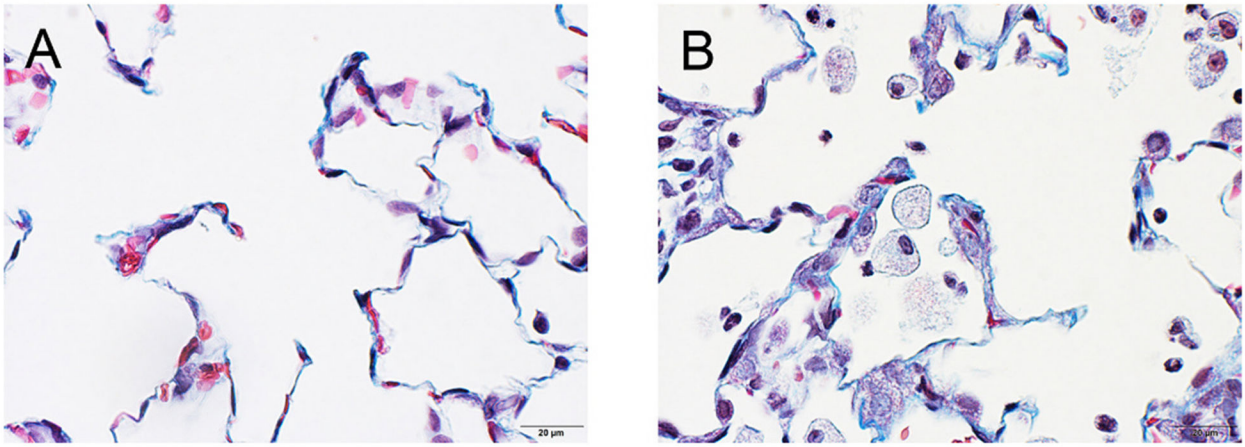


**Fig. 12.**

Trichrome-stained sections of lung. A, PBS negative control. B, MIN-U-SIL positive control. Fibrous connective tissue stains blue. In the MIN-U-SIL-exposed lung, alveolar septa were mildly thickened by blue-staining fibrous connective tissue, indicating mild alveolar septal fibrosis.

**Table 1**

Endotoxin content of FSDs and MIN-U-SIL, and endotoxin dosimetry in rats.

| Sample | [Endotoxin](EU/g dust) | EU/0.5 mg dust/rat* | EU/300 g rat (EU/kg) |
|---|---|---|---|
| 1 | 817.5 | 0.409 | 1.362 |
| 2 | 473.9 | 0.237 | 0.790 |
| 3 | 2558.5 | 1.279 | 4.264 |
| 4 | 116.5 | 0.058 | 0.194 |
| 5 | 655.1 | 0.328 | 1.092 |
| 6 | 759.9 | 0.380 | 1.267 |
| 7 | 170.7 | 0.085 | 0.283 |
| 8 | 275.2 | 0.138 | 0.459 |
| 9 | 96.8 | 0.048 | 0.161 |
| MIN-U-SIL | 172.7 | 0.086 | 0.288 |

* Delivered in 0.3 ml PBS (1.67 mg/ml).

**Table 2**

Element composition of particles ≤2 μm from EDS analysis of FSD 8.

| Particle group | Percentage of particles in sample* | Elements present |
|---|---|---|
| MIN-U-SIL | - | Si, O |
| Group 1 FSD | 53 | Si, O |
| Group 2 FSD | 24.5 | Si, O, Al, K |
| | | Si, O, Al, K, Fe |
| | | Si, O, Al, Fe, Mg, Mn, Ca |
| | | Si, O, Al, K, Mn, Ca, Co |
| Group 3 FSD | 8 | Si, O, Al |
| Group 4 FSD | 6 | Si, O, Fe |
| Group 5 FSD | 5 | O, Mg, Ca |
| Group 6 FSD | 2.5 | O, Fe |
| Group 7 FSD | 0.5 | O, Fe, S |
| Group 8 FSD | 0.5 | Si, O, Mg, Ca |

EDS spectra are shown collectively in Fig. 4 and as separate spectra in Supplementary Figs. 2–12.

*The sample consisted of 200 particles that were subjected to EDS analysis.

## Table 3

XRD analysis of FSDs and MIN-U-Sil using SRM1878b standardization material.

| Sample | % Quartz Primary Result | % Quartz Secondary Result | % Quartz Tertiary Result | % Quartz Average Result |
|---|---|---|---|---|
| 1 | 80.6 | 69.3 | 69.7 | 73.2 |
| 2 | 80.6 | 69.6 | 72.2 | 74.1 |
| 3 | 90.9 | 80.1 | 75.7 | 82.2 |
| 4 | 114 (>95) | 91.0 | 94.0 | 99.6 (>95) |
| 5 | 81.1 | 70.0 | 63.2 | 71.4 |
| 6 | 89.9 | 76.0 | 75.6 | 80.5 |
| 7 | 102 (>95) | 86.7 | 85.5 | 91.3 |
| 8 | 140 (>95) | 95.8 (>95) | 83.1 | 106 (>95) |
| 9 | 111 (>95) | 89.0 | 88.6 | 96.1 (>95) |
| MIN-U-SIL | 92.8 | 91.7 | 90.6 | 91.7 |

Dolomite and tridymite were not detected.

**Table 4**

Overall composition of each sand sample as determined by EDS (atomic %).

| Sample | O | Al | Si | S | K | Ca | Ti | Fe | Sn |
|---|---|---|---|---|---|---|---|---|---|
| 1 | 70.2 | 3.4 | 24.3 | 0.09 | 1.01 | 0.27 | 0.12 | 0.61 | |
| 2 | 69.4 | 4.8 | 24.5 | 0.04 | 1.10 | 0 | 0.06 | 0.07 | |
| 3 | 68.8 | 4.7 | 25.0 | 0.08 | 0.94 | 0.30 | 0.07 | 0.13 | |
| 4 | 67.4 | 1.2 | 29.9 | 0.28 | 0.15 | 0.10 | 0.1 | 0.76 | |
| 5 | 68.6 | 2.9 | 25.4 | 0.10 | 1.10 | 0.70 | 0.1 | 1.20 | |
| 6 | 67.5 | 3.0 | 26.9 | 0.05 | 1.10 | 0.30 | 0.21 | 0.94 | |
| 7 | 71.9 | 1.2 | 24.6 | 0 | 0.68 | 0.96 | 0.04 | 0.54 | |
| 8 | 66.1 | 1.4 | 29.3 | 0.08 | 0.66 | 0.86 | 0.07 | 1.38 | |
| 9* | 69.5 | 1.8 | 25.4 | 0.12 | 0.19 | 1.78 | 0.15 | 1.04 | |
| MIN-U-SIL | 65.5 | 0.6 | 33.7 | 0 | 0 | 0 | 0.14 | 0 | 0.10 |

*Tl (0.07) and Ag (0.04) also were detected in FSD 9.

**Table 5**

Mineral analysis of nine FSD samples and MIN-U-SIL.

| Element | Sample (mg/kg) | | | | | | | | | |
|---|---|---|---|---|---|---|---|---|---|---|
| | **1** | **2** | **3** | **4** | **5** | **6** | **7** | **8** | **9** | **MIN-U-SIL** |
| Aluminum | 2000 | 1700 | 2300 | 700 | 2600 | 1600 | 330 | 1200 | 5400 | 480 |
| Antimony | ND | ND | ND | ND | ND | ND | ND | (3.3)[a] | ND | ND |
| Arsenic | ND | ND | ND | ND | ND | ND | ND | ND | ND | ND |
| Barium | 55 | 120 | 59 | 140 | 310 | 31 | 12 | 54 | 290 | 79 |
| Beryllium | (0.19)[a] | (0.12)[a] | ND | ND | (0.17)[a] | ND | ND | (0.26)[a] | ND | ND |
| Cadmium | 0.87 | (0.55[a] | 1.0 | 2.1 | 1.7 | (0.64)[a] | (0.32)[a] | 2.6 | 1.2 | ND |
| Calcium | 4500 | 1200 | 3300 | 1200 | 7000 | 1800 | 6800 | 11,000 | 16,000 | 220 |
| Chromium | 5.7 | 3.7 | 4.9 | 14 | 7.6 | 7.1 | 3.1 | 14 | 8.7 | (0.61)[a] |
| Cobalt | 2.7 | 3.2 | 2.1 | 1.8 | 4.0 | 1.9 | (1.1)[a] | 8.7 | 2.8 | ND |
| Copper | 5.2 | 3.1 | 3.7 | 11 | 7.5 | 3.1 | 3.9 | 30 | 14 | (1.8)[a] |
| Iron | 4900 | 3100 | 4400 | 7100 | 8600 | 3800 | 2800 | 14,000 | 5700 | 440 |
| Lanthanum | 2.3 | 21 | 3.7 | ND | 1.7 | 3.7 | ND | ND | ND | (0.45)[a] |
| Lead | 6.3 | 9.1 | (4.4)[a] | (4.8)[a] | (4.3)[a] | (5.1)[a] | (2.8)[a] | 14 | (3.2)[a] | ND |
| Lithium | 2.1 | 1.9 | 2.2 | 1.7 | 5.3 | 2.4 | 1.7 | 2.1 | 3.7 | 1.7 |
| Magnesium | 850 | 160 | 360 | 320 | 2500 | 430 | 2300 | 3900 | 3100 | 48 |
| Manganese | 64 | 35 | 68 | 52 | 230 | 46 | 110 | 1200 | 67 | 2.9 |
| Molybdenum | (0.87)[a] | ND | (0.92)[a] | (2.2)[a] | ND | ND | ND | (1.8)[a] | (1.5)[a] | ND |
| Nickel | 2.8[b] | 2.7[b] | 2.1[b] | 8.3[b] | 8.2[b] | 2.2[b] | 1.7[b] | 12[b] | 5.1[b] | ND |
| Phosphorus | 110 | 69 | 94 | (42)[a] | 450 | 130 | 350 | 440 | 270 | (39)[a] |
| Potassium | 370[b] | 320[b] | 380[b] | 110[b] | 700[b] | 290[b] | 170[b] | 520[b] | 240[b] | 91[b] |
| Selenium | ND | ND | ND | ND | ND | ND | ND | ND | ND | ND |
| Silver | ND | ND | ND | ND | ND | ND | ND | ND | ND | ND |
| Strontium | 6.9 | 5.8 | 6.3 | 8.1 | 25 | 12 | 11 | 16 | 190 | 8.9 |

| Element | Sample (mg/kg) | | | | | | | | | |
|---|---|---|---|---|---|---|---|---|---|---|
| | 1 | 2 | 3 | 4 | 5 | 6 | 7 | 8 | 9 | MIN-U-SIL |
| Tellurium | ND | ND | ND | ND | ND | ND | ND | ND | (6.6)[a] | ND |
| Thallium | (3.7)[a] | ND | ND | ND | ND | ND | ND | ND | ND | ND |
| Tin | ND | ND | ND | ND | ND | ND | ND | ND | ND | ND |
| Titanium | 59 | 110 | 48 | 20 | 65 | 59 | 10 | 34 | 340 | 6.7 |
| Vanadium | 15 | (9.2)[a] | (9.5)[a] | ND | 17 | (8.7)[a] | (5.6)[a] | 19 | 20 | ND |
| Yttrium | 7.2 | 6.7 | 5.0 | 4.3 | 6.2 | 3.5 | 2.7 | 4.4 | 5.4 | 2.7 |
| Zinc | 16 | 18 | 15 | 110 | 44 | 15 | 9.5 | 56 | 32 | 14 |
| Zirconium | 3.5 | 4.2 | 3.2 | 9.3 | 2.7 | 2.0 | 1.1 | 2.6 | 8.3 | 1.4 |
| Total mg/kg | 12,989 | 6903 | 11,073 | 9862 | 22,590 | 8253 | 12,927 | 32,535 | 31,710 | 1438 |

ND, not detectable or at the limit of detection. (), estimated value between the LOD and the LOQ.

[a]Detected at a value below the LOQ.

[b]Detected in the media blank.

**Table 6**

Histopathology scores following i.t. instillation of PBS, MIN-U-SIL and nine FSDs.[1]

| Dust Dose | Treatment | | | | | | | | | | |
|---|---|---|---|---|---|---|---|---|---|---|---|
| | **PBS** | **MIN-U-SIL** | **1** | **2** | **3** | **4** | **5** | **6** | **7** | **8** | **9** |
| Histiocytic and neutrophilic inflammation in alveoli | | | | | | | | | | | |
| Low | 0 (6) | 0 (2) | 0 (4) | 0 (4) | 0 (3) | 0 (3) | 0 (3) | 0 (3) | 0 (4) | 0 (4) | 0 (4) |
| | | 4 (2) | | | | 4 (1) | | | | | |
| High | - | 4 (1)* | 0 (4) | 0 (4) | 0 (3) | 0 (4) | 0 (3) | 0 (2) | 0 (3) | 0 (3) | 0 (4) |
| | | 5 (1) | | | | | 4 (1) | 4 (1) | | | |
| | | 6 (1) | | | | | | | | | |
| Alveolar histiocytosis | | | | | | | | | | | |
| Low | 0 (3) | 0 (3) | 0 (1) | 2 (1) | 0 (2) | 0 (1) | 3 (1) | 0 (3) | 0 (3) | 0 (1) | 0 (1) |
| | 2 (1) | 2 (1) | 4 (1) | 4 (2) | 4 (1) | 2 (1) | 4 (2) | | 4 (1) | 4 (3) | 3 (1) |
| | 4 (2) | | 5 (2) | 5 (1) | | 3 (1) | | | | | 4 (1) |
| | | | | | | 5 (1) | | | | | 5 (1) |
| High | - | 0 (3) | 0 (2) | 0 (1) | 0 (1) | 0 (1) | 0 (2) | 0 (2) | 0 (2) | 0 (2) | 2 (1) |
| | | | 2 (1) | 2 (1) | 2 (1) | 4 (2) | 3 (1) | 3 (1) | 2 (1) | 5 (1) | 3 (2) |
| | | | 4 (1) | 3 (1) | 3 (1) | 5 (1) | 4 (1) | | | | 6 (1) |
| | | | | 5 (1) | | | | | | | |
| Alveolar epithelial cell hypertrophy and hyperplasia | | | | | | | | | | | |
| Low | 0 (6) | 0 (2) | 0 (4) | 0 (4) | 0 (3) | 0 (3) | 0 (3) | 0 (3) | 0 (4) | 0 (3) | 0 (4) |
| | | 2 (2) | | | | 3 (1) | | | | 2 (1) | |
| High | - | 0 (1) | 0 (4) | 0 (4) | 0 (3) | 0 (4) | 0 (3) | 0 (3) | 0 (3) | 0 (3) | 0 (4) |
| | | 4 (1) | | | | | | | | | |
| | | 5 (1) | | | | | | | | | |
| Fibrosis diagnosed by trichrome | | | | | | | | | | | |
| Low | 0 (6) | 0 (3) | 0 (3) | 0 (3) | 0 (3) | 0 (3) | 0 (2) | 0 (3) | 0 (4) | 0 (4) | 0 (3) |
| | | 4 (1) | 4 (1) | 4 (1) | | 2 (1) | 3 (1) | | | | 4 (1) |
| High | - | 4 (2)* | 0 (4) | 0 (4) | 0 (1)* | 0 (1)* | 0 (3) | 0 (3) | 0 (3) | 0 (4) | 0 (2) |
| | | 5 (1) | | | 3 (3) | 4 (3) | 5 (1) | | | | 2 (1) |
| | | | | | | | | | | | 5 (1) |

[1] Values are the pathology scores (severity + distribution). *n* numbers in parentheses.

* Significantly different from PBS control.